CHAPTER 2

Design, Fabrication and Characterization of SnO_2 Based Thick Film Sensor Array

Present chapter deals with the study of electronic properties of SnO_2 viz. bulk and surface properties. It also discusses the gas sensing mechanism in brief. Finally, the design, fabrication and characterization of the SnO_2 based gas sensor array have been described. The fabricated sensor array has been used for further analysis of individual and mixture of gases/odors in Chapter-3 and Chapter-5 respectively.

2.1 Introduction

Different commercial gas detectors are gas selective in nature and costly to manage. Thick film technology provides a cost effective solution in this regard as described in detail in previous chapter. Thick film gas sensors with tin-oxide as a base material have proved their ability for gas detection and have shown sensitivity to multiple gases [Oyabu *et al.* (1982); Watson (1984)]. The integration of multiple sensor elements doped with different dopants like Pd, Pt, ZnO, etc. on a common substrate produces different patterns for different gases/odors enabling them to be utilized in e-nose system for gas sensing application. Present chapter describes the design, fabrication and characterization of SnO_2 based thick film sensor array used for various studies in the present work.

2.2 Crystalline Structure and Electronic Properties of SnO_2

Tin (atomic number 50) is a main group metal in group 14 of the periodic table and lies at the boundary between metals and non-metals. It is a malleable, ductile and highly crystalline silvery-white metal and shows chemical similarity to neighboring group-14 elements, germanium and lead. It has two possible oxidation states, +2 and a slightly more stable +4 in compound form. The divalent and trivalent oxidation states have been designated as stannous and stannic respectively. The present work is concerned with Sn (IV) oxide which is called tin oxide or stannic oxide or stannic anhydride with a chemical formula SnO_2.

SnO_2 is n-type semiconductor with wide band gap of 3.6 eV at 300 K. The n-type behavior is mainly due to the non stoichiometric or oxygen deficient structure [Robertson(1979); Kohl (1990); Kilic *et al.* (2002)]. SnO_2 exhibits the rutile structure with space group P4/mnm. It has tetragonal structure with two tin and four oxygen atoms. Each tin oxide atom is surrounded by octahedron of six oxygen atoms whereas each oxygen atom is surrounded by three tin atoms at the corners of almost equilateral triangle with lattice parameters a=b=4.737 A° and c=3.186 A°, internal parameter u= 0.307 A°. Atomic positions are determined by the c/a ratio and the internal parameter u [Barbarat (1997)]. Fig. 2.1 shows the crystalline structure of SnO_2 unit cell.

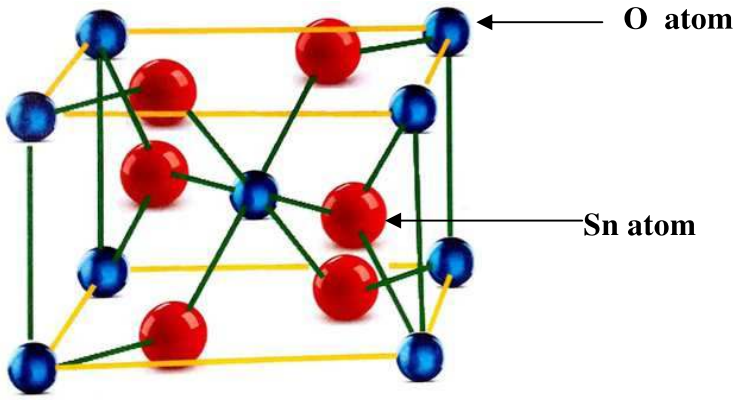

Fig. 2.1 Crystalline structure of SnO_2 unit cell [Chaudhary (2013)]

SnO_2 has some good features such as low cost, simple design and has appreciable sensitivities to the wide varieties of combustible, toxic and pollutant gases/odors. Though the pure SnO_2 is free of surface states but electron donors (like adsorbed hydrogen) or electron acceptor (like oxygen) causes the formation of surface states in the wide band gap. This wide band gap is responsible for the electron exchange with the bulk SnO_2. Furthermore, a space charge region can be easily modified by changing the donor or acceptor concentrations. The thermal ionization in non-stoichiometric SnO_2 is very easy because the defect levels lie just below the conduction band minimum. There exist two conduction band levels with activation energy of 100 meV and 300 meV respectively [Mizokawa *et al.* (1975)] for the one 1-state of Sn and O. Fig. 2.2 shows the band diagram for SnO_2 and the projection of the density of states [Barbarat *et al.* (1997)]. A large contribution of Sn states is found at the bottom of valance band -7 eV and -5 eV. Bonding between Sn and O is dominated

by the p-states of the latter. Each anion in a unit cell is found to be bonded to the cations in a planer-trigonal configuration in such a way that the oxygen p-orbitals contained in the four atom plane *i.e.* p_x and p_y define bonding plane. Consequently, the oxygen *p* orbitals perpendicular to bonding plane *i.e.* p_z orbitals have non-bonding character and expected to form upper valence levels [Barbarat *et al.*(1997); Ivanov (2004)].

SnO_2 sensors are typically operated at temperature between 200 °C and 400 °C. If the conduction processes are independent then the conductivity (σ_{tot}) can be defined as the sum of electronic conductivity ($\sigma_n + \sigma_p$) and ionic conductivity (σ_{ion}) *i.e.*

$$\sigma_{tot} = \sigma_n + \sigma_p + \sum \sigma_{ion,I} \approx \sigma_n + \sigma_p \tag{2.1}$$

The resistance of homogenous bulk material with bulk conductivity σ_b can be calculated as:

$$R_b = \frac{l}{\sigma_b A} \tag{2.2}$$

with $\sigma_b = \sigma_n + \sigma_p = n\mu_n e + n\mu_p e$, where l is length and A is cross sectional area of the bulk material.

The n-type behavior of SnO_2 is associated with oxygen deficiency in the bulk, The donors are single and double ionized oxygen vacancies with donor levels E_{D1} and E_{D2} located around 0.03 eV and 0.15 eV below the conduction band edge as shown in Fig. 2.3. The extrinsic donors in the SnO_2 are multistep donors. The bulk conductivity is collectively determined by the donor and acceptor energy levels, concentrations and the temperature [Fonstad *et al.* (1971), Hahn (2002); Chaudhary (2013)].

2.3 Surface Properties of SnO_2

Gas sensing by the tin oxide is basically based on surface phenomenon (chemical and physical). As the sensors are exposed to the gas, the interaction of oxide surface with gas causes the surface reactions such as chemisorptions, reduction/oxidation and/or catalysis to take place which results in change in the concentration of conduction electrons and hence the conductivity of the gas sensing material. It is necessary to understand the surface reaction of semiconductors with gases with both chemical and physical point of view [Korotcenkov (2004)].

From chemical point of view, the surface molecular model considers that the sensor surface can be divided into different sites of varying conductivity. These

reactive sites are surface atoms with unoccupied or unsaturated orbital (dangling bonds), surface atoms with unsaturated co-ordination spheres, crystallographic steps, intersection and interstitials or superstructures.

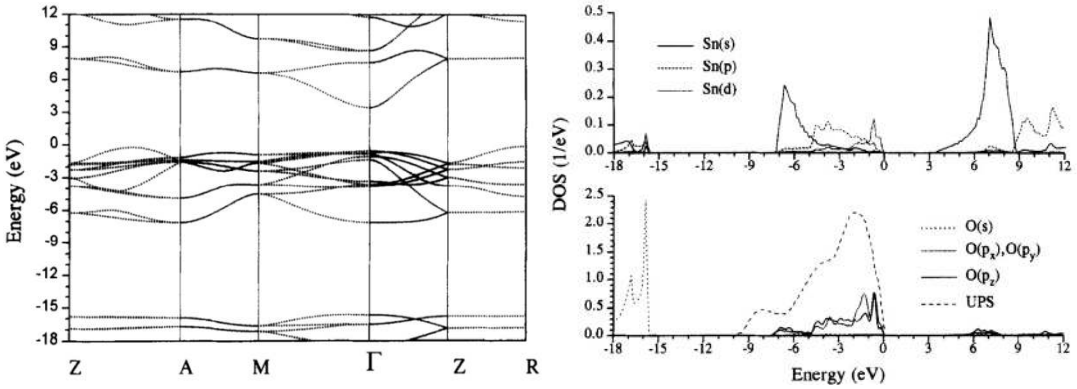

Fig. 2.2 Band diagram for SnO_2 (left) and the projection of the density of states (right) [Barbarat *et al.* (1997)]

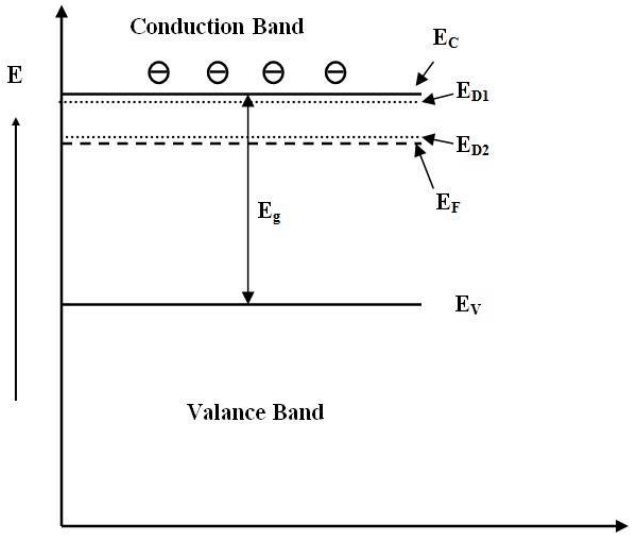

Fig. 2.3 Schematic band diagram of SnO_2, donor level E_{D1} =0.03 eV, E_{D2} =0.15 eV

From physical point of view, the band model considers the interruption of the crystal periodicity at the surface generally result in localized energy levels which act as acceptor or donor states for exchanging or sharing electrons with non-localized energy bands in the bulk of the solid. The electronic properties of solid are greatly influenced by these energy levels existing in the band gap. The surface effects can result from non-ideal stoichiometry composition or bulk defects (intrinsic) or may be due to unintentional impurity addition.

2.3.1 Adsorption

All surface processes are driven by the fundamental phase of adsorption of foreign atoms or molecules which causes essential rearrangement of surface chemical bonds and consequently the variation of the surface state density and the surface potentials. '*Adsorption' is the process producing net accumulation of substance at the common boundary of two contiguous phases* [Burwel (1976)]. Adsorption can occur on all types of surfaces and basically five types of interaction may exist viz. gas-solid, liquid-solid, liquid-liquid, solid-solid and gas-gas. Adsorption is always exothermic in all these interactions [Chaturvedi (2000)].

Adsorption on solid is a complex phenomenon. The catalytic surface of SnO_2 consists of a large number of active sites on which gases are adsorbed. The adsorbed molecules of gas may be independent of each other or it may interact with the nearest neighbors or with more distant neighbors which may be mobile or immobile.

There are two types of adsorption *i. e. physisorption* and *chemisorptions*.

(i) *Physisorption (Physical adsorption)*:

Physisorption describes an adsorption process without any change in the geometric structure and in the electrical properties of free particles or free surfaces. In this type of adsorption, the adsorbate adheres to the surface through Van der Waals interactions which are weak interactions. The perturbation of the electronic states of adsorbent and adsorbate is minimal. The elementary step in physisorption from a gas phase does not involve activation energy. This adsorption usually takes place at very large distance '*r*' from the surface (adsorbent). The gas molecules which approach to the surface are slightly polarized and induce a weak dipole in the adsorbent. The physical adorption potential can be characterized by a two-particle model by applying the Lennard-Jones potential which describes the attractive and repulsive forces between two particles as follows [Atkins (1990)]:

$$V = E_{attr} + E_{rep.} \propto 4\in\left[-\left(\frac{a}{r}\right)^{6} + \left(\frac{a}{r}\right)^{12}\right] \tag{2.3}$$

where, a = distance between the interacting particles;

r = atomic distances; and $\in$ = depth of potential cavity.

Physical adsorption is the first step in the interaction between a gas molecule and surface of a solid. This type of adsorption consists of monolayer, multilayer or condensation of the adsorbate in the liquid form residing in the tiny capillaries of the

adsorbent [Chaturvedi (2000)]. Small binding forces (~2eV) are involved which causes physiosorption to totally disappear at elevated temperature [Kennedy (2004)]. So, the physiosorption is characterized by a high surface coverage with gaseous molecules at low temperature and low coverage at high temperatures. For adsorption up to one monolayer this coverage θ is defined as:

$$\theta = \frac{N}{N_t} \tag{2.4}$$

where, N= number of molecules adsorbed per surface unit

N_t = total number of adsorption sites.

(ii) *Chemisorption*:

Chemisorption involves a chemical reaction between the surface and the adsorbate which adheres to the surface. It is characterized by strong interactions which lead to higher bonding energy between surface and the adsorbate molecules. These bonding energies are of similar strength as for chemical bonds. There are two basic types of chemisorptions mechanisms [Hagan (1996)]:

(a) Molecular and associative chemisorptions, where all atomic bonding are refrained in the adsorbed molecule.

(b) Dissociative chemisorptions, where the bonding of the adsorbed molecules undergoes decomposition and the resulting individual molecule fragments are bonded on the metal oxide surface.

Mostly, the molecular chemisorptions are obtained if the molecules have free electrons or multiple bonding. On the other hand molecules with single bonding react via a dissociative chemisorption. Fig. 2.4 shows the potential diagram of a dissociative chemisorption of oxygen on tin dioxide [Hagan (1996)].

This potential diagram consists of two overlapping curves. The flat curve corresponds to the physisorption of the molecular oxygen. The molecular oxygen runs along the curve 1 over the physisorption status to intercept at point *A* with curve 2 of the atomic oxygen, where the dissociation of oxygen starts. An activation barrier separates the chemisorption status from the physisorbed status.

Both types of status can be distinguished via the bonding energy between the adsorbent and the adorbate. If the energy is above 0.5 eV per particle, it is chemisorptions and this effect is normally thermally activated.

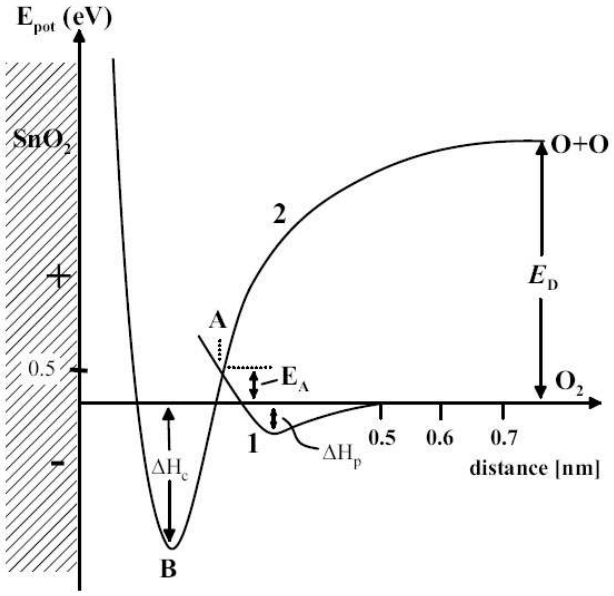

Fig. 2.4 Potential energy and atomic distance at the adsorption of a dissociative chemisorption oxygen on tin oxide [Kennedy (2004)]

Bonding becomes weaker after a transition state O-O which leads to formation of new Sn-O bonding where both atoms are bonded at a defined distance from the surface. ΔH_p is the free energy after physisorption and ΔH_C after chemisorption; E_D is the dissociation energy for the oxygen molecule and E_A the activation energy for the adsorption. The chemisorbed oxygen is located closest to the metal-oxide surface at *B* with the lowest potential energy. The dissociative chemisorptions always increase the amount of chemical bonding so that the overall process becomes exothermic. The whole process is shown schematically in Fig. 2.5.

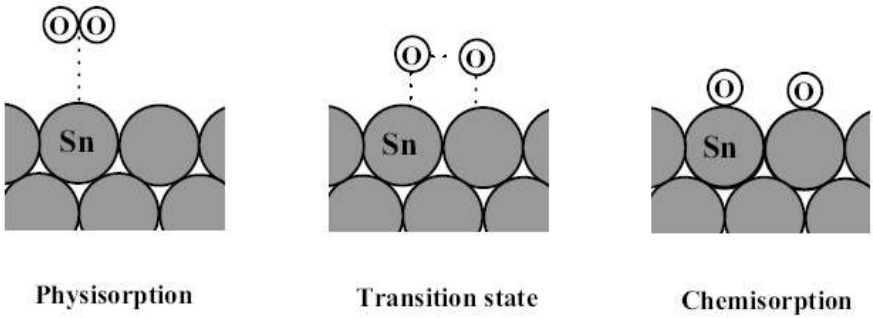

Fig. 2.5 Adsorption process of oxygen on a SnO_2 surface. Two Sn-O bondings are developed from one chemical bonding in the oxygen molecule on the surface [Kennedy (2004)]

2.3.2 Adsorption Isotherms [Srivastava *et al.* (1994); Reichel (2005); Chaudhary (2013)]

The free gas and the adsorbed gas on the surface are in dynamic equilibrium and the fractional coverage (θ) of the surface depends on the pressure of overlying gas. The dependence of θ on the pressure at constant temperature is called adsorption isotherms. It provides a framework for describing the extent and the strength of the adsorption of molecule on the surface and also the basis for representing the kinetics of the surface catalyzed reactions. The adsorption rate of the gaseous molecule is proportional to gas pressure and to the number of unoccupied adsorption sites (1- θ) according to following equation.

$$\frac{d\theta}{dt} = K_{ads}(1-\theta)P_{gas} \tag{2.5}$$

with the adsorption constant $K_{ads} = Ae^{\left(-\frac{E_A}{KT}\right)}$

The desorption rate is proportional to the number of occupied sites θ according to (2.6)

$$\frac{d\theta}{dt} = K_{des}(\theta) \tag{2.6}$$

where, desorption constant $K_{des} = B.e^{(-E_{Diss}/KT)}$

The net adsorption rate can be described as shown in (2.7)

$$\frac{d\theta}{dt} = K_{ads}(1-\theta)P_{gas} - K_{ads}(\theta) \tag{2.7}$$

with a resulting equilibrium coverage θ for $d\theta/dt$ =0

$$\theta = \frac{P_{gas}}{P_{gas} + \frac{K_{des}}{K_{ads}}} \tag{2.8}$$

where, $\theta = f(P_{gas}, T)$. Equation (2.5) represents the Langmuir Isotherms. It states that the adsorption and desorption processes not only depends on the nature of the adsorbate and adsorbent but also on the partial pressure (P_{gas}) of the adsorbate and the temperature (T). The isotherm is applicable only for monolayer adsorption and desorption and is acceptable for desorption at low pressure only and holds good for physical adsorption and homogenous surfaces. Brunauer, Emmet and Teller (BET) [Brunauer *et al.* (1938)] proposed a new model called BET isotherm which is valid for multilayer adsorption and desorption, and is given by:

$$\frac{P}{v(P_s - P)} = \frac{1}{v_m c} + \frac{(c-1)c}{v_m}\frac{P}{P_s} \tag{2.9}$$

where, P_s= saturation pressure of vapor; c = constant; P = partial pressure and v_m = total volume available for adsorption

Freundlich adsorption Isotherm [Chaturvedi *et al.* (2000)] represents a logarithmic change. It correlates the amount of molecule adsorbed to the concentration of the gas as shown in (2.10)

$$m = KC^b \tag{2.10}$$

where, m = amount adsorbed; C = concentration of gas; K = adsorption coefficient and b = constant ($0<b<1$).

This equation is an empirical one and holds good for physical as well as chemical adsorptions. The Freundlich adsorption isotherm is considered more appropriate for thick film gas sensors because the large recovery time of these sensors indicates that the sensing mechanism include both physical as well as chemical adsorption to take place at the sensor surface. The Langmuir adsorption mechanism has not been considered because it is valid only for physical adsorption. BET adsorption is valid for multilayer condensation which seems suitable for sensor surfaces [Srivastava (1994)].

2.3.3 Gas Sensing Mechanism in SnO_2 [Srivastava (2011); Chaudhary (2013)]

The gas sensing phenomenon in tin oxide can be described via chemisorptions process combined with a charge transfer process at the n-type semiconductor surface. At room temperature, the coverage of physisorbed molecules is less than one monolayer. This process is accomplished by weak van der Waals forces. The oxygen molecules are physisorbed below 100 °C while physisorption desorption disappears above 100 °C and dissociative chemisorptions take place. In the latter case, oxygen molecules are dissociated via a chemisorption process. Firstly, oxygen is connected via dipole bonding to the semiconductor surface atoms. Under this condition, electrons are removed from the semiconductor surface via a charge transfer mechanism followed by the formation of chemical bonds with the semiconductor surface atoms. The e-concentration near the semiconductor surface varies with density and occupancy of surface acceptors and donors. The effect of charge transfer on the electronic properties of the semiconductor is shown in Fig. 2.6.

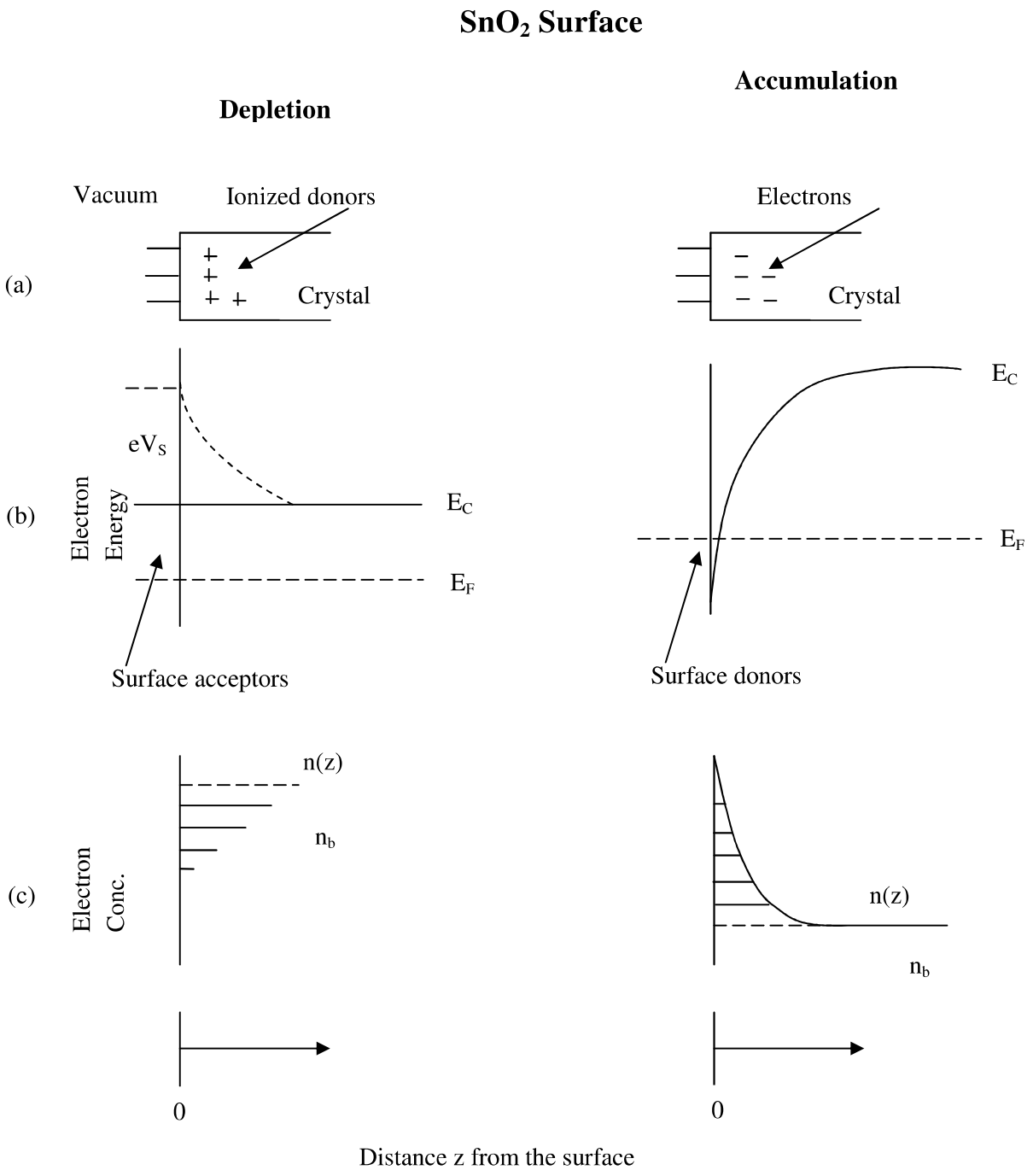

Fig. 2.6 Surface charge layers on the surface of *n*-type semiconductor with a wide band gap (a) Distribution of charges (b) Band scheme near conduction band edge (c) Concentration n(z) of electrons in the conduction band

Due to high electro negativity of oxygen atom, its adsorption at the surface leads to an oxidation of semiconductor surface and a reduction of the gas to which the surface is exposed. A transition of electrons from the conduction band E_c to surface acceptor states creates a negative charge at the surface. This negative charge layer is compensated with a positive counter charge in the solid which is formed in the bulk (donor ions) resulting into space charge region. According to the schottky approximation [Morrison (1982)] this region is characterized by total exhaustion of mobile charge carriers (all mixed to the surface) and therefore called depletion layer. Between these two space charge layers, an electric field is developed and a measure of this electrical field is the Debye length L_D which is defined as in equation (2.11)

$$L_D = \sqrt{\frac{\varepsilon_r \varepsilon_o KT}{e^2 N_{(v)}}} \tag{2.11}$$

Equation (2.11) gives the relation between Debye length L_D (the extension of the space charge region in the bulk) and concentration of the free charge carriers $N_{(v)}$. The chemisorbed species can have an electrical charge and consists of one or more atoms. The various species of oxygen relevant to the surface reaction is shown in Fig. 2.7.

At the temperature above 450 K, O^- ions are found as prevailing species. Reactivity of O^-_{ads} is higher than that of O^-_{2ads}. O^{2-}_{ads} is unstable and has to be stabilized by the Madelung potential of the lattice *i. e.* on a lattice site. Adsorbed O^{2-}_{ads} and O^-_{ads} and also exposed oxygen atoms on step sites are classified as electrophilic reactants which preferentially attack the C-C double bond of the adsorbates abstracting electron whereas the 'nucleophilic' O^{2-} ions bound within the lattice at the surface react with activated hydrogen or dehydrogenated hydrides and hydrocarbons. Activation means excitation of a bond and as possible consequence ionization, dissociation or formation of radicals [Mishra (1996), Srivastava (2011)].

On SnO_2 films, the following reaction take place with increasing temperature

$$O^-_{2ads} + e^- \rightarrow 2O^-_{ads} \tag{2.12}$$

When a metal oxide crystal such as SnO_2 is heated at a particular high temperature in air, oxygen is adsorbed on the crystal surface with negative charge. Then, donor electrons in the crystal surface are transferred to the adsorbed oxygen which leave

positive charge in the space charge layer. This creates surface potential which serves as potential barrier against electron flow.

Though several attempts have been made to describe the gas sensing mechanism of tin oxide still the mechanism is not fully understood [Torvela *et al.* (1988), Mishra (1996)]. The sensing mechanism has been generally described chemisorptions of atmospheric oxygen at SnO_2 surfaces followed by the extraction of the electrons from the bulk at the elevated temperature. Due to this process the surface of tin oxide gets depleted of electrons as the electrons get trapped.

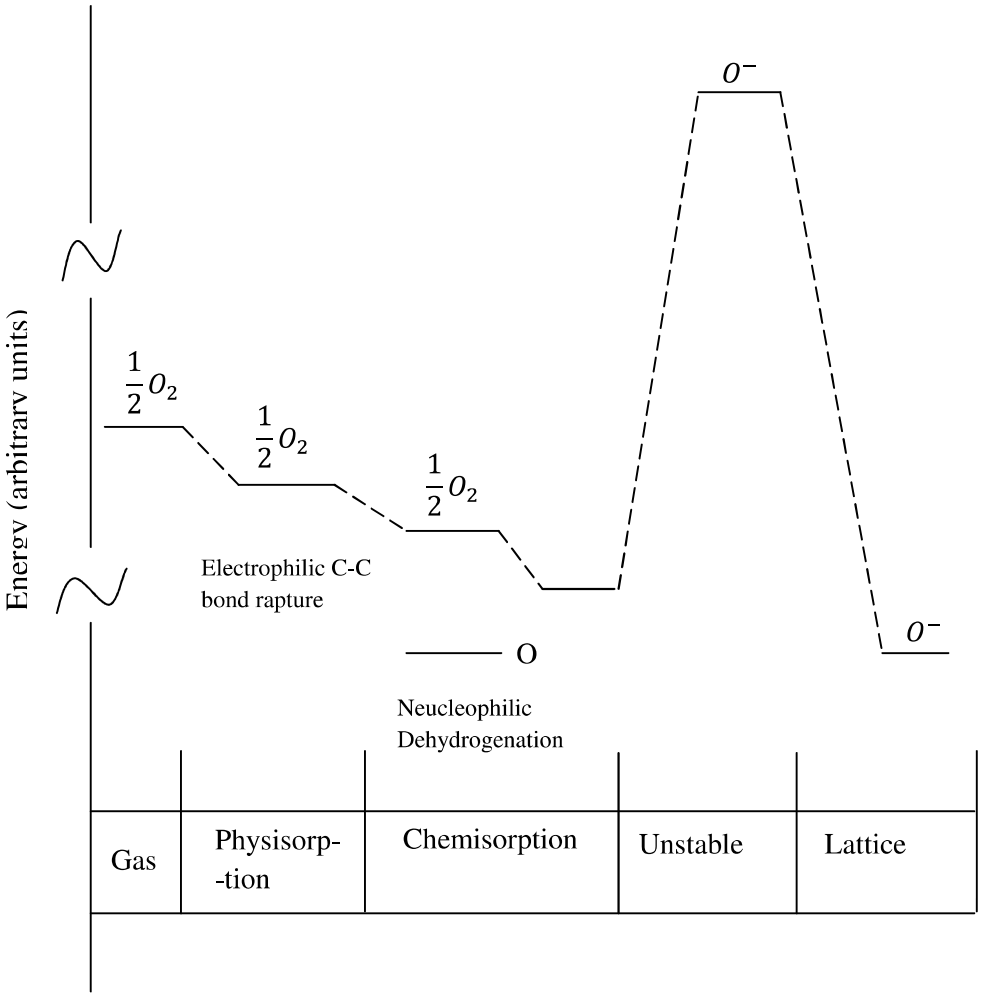

Fig. 2.7 Energy diagram of various oxygen species in the gas phase adsorbed at the surface and bound within the lattice of a binary metal oxide [Kohl (1990)].

The exposure of reducing gas like hydrogen on this oxygen chemisorbed surface causes the reduction of adsorbed oxygen and reaction with the hydrogen molecules via the following step [Drauglis *et al.* (1969)]:

$$H_2(g) + O(ads) = H_2O(g) \tag{2.13}$$

The most accepted model for the operation of a dopant free-powder based semiconductor gas sensor has been reported by Morrison, Heiland and Gopel [Morrison (1982); Heiland (1982); Gopel (1985)]. Fig. 2.8 shows the model of inter-grain potential barrier in the absence and presence of gases.

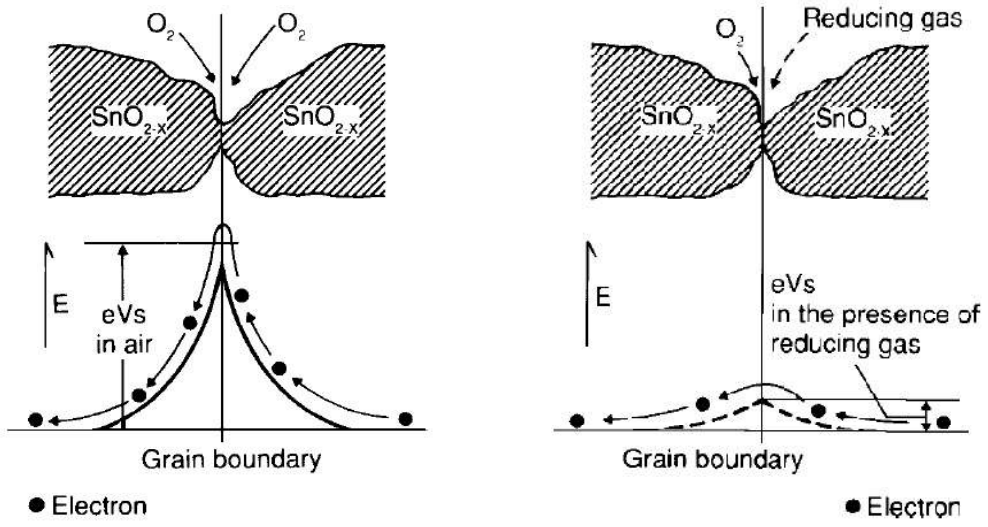

Fig. 2.8 Model of inter-grain potential barrier in the absence of gases (left) and in the presence of gases (right) [Gupta (2008)]

When SnO_2 is heated at a certain high temperature in air, oxygen is adsorbed on the crystal surface with a negative charge. Then donor electrons in the crystal surface are transferred to the adsorbed oxygen, resulting in leaving positive charges in a space charge layer. Thus, surface potential is formed to serve as a potential barrier against electron flow (Fig. 2.8 (left)). Inside the sensor, electric current flows through the conjunction parts (grain boundary) of SnO_2 micro crystals. At grain boundaries, adsorbed oxygen forms a potential barrier which prevents carriers from moving freely. The electrical resistance of the sensor is attributed to this potential barrier. In the presence of a deoxidizing gas, the surface density of the negatively charged oxygen decreases, so the barrier height in the grain boundary is reduced (Fig. 2.8 (right)). The reduced barrier height decreases sensor resistance.

In SnO_2 sensors, the conductivity increases in the presence of reducing gases (such as CO) and decreases in the presence of an oxidizing gas (such as O_2). Gases

with low electro negativity act as donor that transfer electrons to the semiconductor and cause increase in charge density and reduce the surface potential barrier, depth of the depletion region and work function resulting in increase in the conductivity. Some reducing gases like CO and hydrocarbons do not interact in direct manner rather react with adsorbed oxygen.

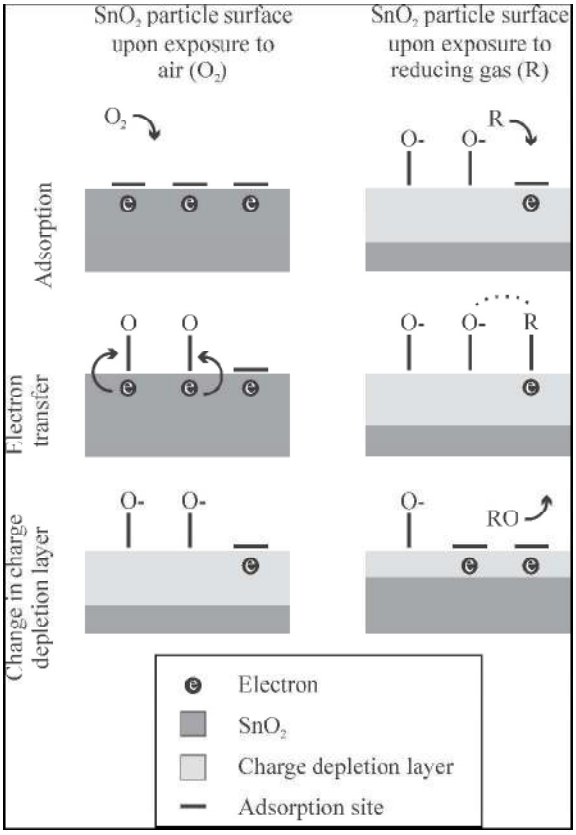

Fig. 2.9 Schematics indicating the mechanisms leading to SnO_2 sensor response to oxidizing and reducing gases [Miller (2006)]

Oxidizing gases act as acceptors, trapping electrons from the semiconductor at the surface sites. The process is reversed *i.e.* the decrease in the charge concentration will increase the surface potential barrier, depth of depletion region and work function which ultimately result in decrease of the conductivity of the semiconductor [Reichel (2005); Srivastava (2011)]. The general steps of interaction mechanism of SnO_2 sensor with oxidizing and reducing gases can be understood in the simplest way as shown in Fig. 2.9.

2.3.4 Doping

Generally the metal oxide sensors are not very selective and their sensitivity is very low at room temperature. The sensitivity and the selectivity of these sensors can be substantially improved by adding a low concentration of additives in its volume which are termed as dopant. A dopant is a material that expedites the rate of chemical reaction without itself getting changed. It does not change the free energy of the reaction but lowers the activation energy. Also, it does not cause sensor poisoning. Catalytic active materials such as Pt, Pd, Cd, Ti, Zn, Pb, Au or Ag are often added in traces as dopants. Increased selectivity, sensitivity, signal stability, reproducibility and reduced response and recover time of the sensor are among the possible changes that can be achieved by adding such dopants [Yamazaoe (1991)]. They play role of added surface sites for adsorbents. Thus, the dopant can influence a reaction in two ways. Firstly, it can increase the concentration of reaction partners at the reaction sites thereby increasing the reaction probability. Secondly, it can decrease the activation energy of the chemical reaction and thereby open new reaction paths without any change in the free energy of chemical reaction.

The working principal of additive modified SnO_2 materials is still not completely understood. Two general models [Yamazoe *et al.* (1991)] of the gas sensing mechanism for such materials have been proposed viz. *chemical* and *electronic* sensitization. Both models assume that small doping crystallites are located on the surface of a much bigger grain of SnO_2. The distribution of these small dopants is assumed to be mostly homogenous on the tin oxide surface a shown in Fig. 2.10.

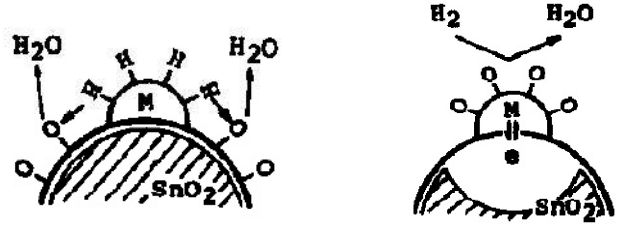

Fig. 2.10 Effect of doping on SnO_2 as Chemical (left) and Electronic (right) Sensitization [Yamazoe (1991)]

The chemical model considers the spillover mechanism which is attributed to the presence of metallic clusters at the surface of SnO_2 grains. The catalyst forces a dissociation of reactants and thereby increases the concentration of reactive particles at the surface. The electronic sensitization considers Fermi level control which is

related to an electronic interaction in which the oxygen adsorption on the catalyst removes electrons from the catalyst which in turn removes electrons from the supporting semiconductor thus controlling the energy of the Fermi level and influencing the band bending in the tin oxide grain.

Summary of some reported dopants used for SnO_2 and the gases to which they show good sensitivity has been shown in Table 2.1

Table 2.1 Summary of some reported dopants used for SnO_2 and the gases to which they show good sensitivity

Dopants	**Target gas detected**	**References**
Pd	CO, LPG, CH_4	Menini *et al.* (2004); Chakarborty *et al.* (2007); Chuadhary (2013); Srivastava (2011)
Pt	CO, LPG,	Cabot *et al.* (2000); Menini et al (2004)
CuO, ZnO	CO, H_2, H_2S, NO, CO_2	Yu *et al.* (2001); Liu *et al.* (2003); Chowdhuri *et al.* (2003); Zhang *et al.* (2000)
Sb	Alcohols, CO	Liu *et al.* (2003); Mishra *et al.* (2002)
La_2O_3	CO_2, C_2H_4O, CO	Kim *et al.* (2000); Kugishima *et al.* (2006); Choi *et al.* (2013)
CeO_2	CH_4, Acetone	Butta *et al.* (1992); Bagal *et al.* (2012)
Cd	H_2	Tianshu *et al.* (1999)
Rh	Acetaldehyde	Shimizu *et al.* (2000)
Au	CO	Neli et al (2000); Wang *et al.* (2006)
Ag	H_2, H_2S, propane	Zhang *et al.* (1997); Carbajaj-Franco *et al.* (2000)

2.3.5 Sensor Operating Temperature

The tin oxide sensors show negligible sensitivity at room temperature. For improving the sensitivity the sensor is operated at elevated temperature. By varying the operating temperature of the sensor, it is possible to vary its sensitivity and selectivity towards the specific gas/odor. This special attribute of SnO_2 gas sensors can be exploited to maximize the sensor signal to each target gas and discern between two target gases [Lee *et al.* (1999)]. The adsortption, reaction and desorption of gases on the sensor surface depends on the operating temperature. The optimum operating temperature is

generally mentioned by the paste manufacturer or it is optimized manually for gases/odor under test.

2. 4 Fabrication of Gas Sensor Using Thick Film Technology

This section reviews the thick-film processes used for fabricating the desired sensors. All the implemented processes are briefly explained in this section.

A thick-film circuit generally consists of layers of special inks (or pastes) deposited onto an insulating substrate (like alumina (96%), ceramic). Screen-printing is possibly one of the oldest forms of graphic art reproduction and is one key factor which distinguishes a thick film circuit form other. The deposition process for a thick-film circuit is essentially identical to that used for traditional silkscreen printing. The measure differences lie in the screen materials and the degree of sophistication of the screen printing machine. A typical thick-film screen consists of a finely woven mesh of nylon, polyester or stainless steel. It is mounted under tension on a metal frame. The mesh is coated with a ultra-violet (UV) sensitive emulsion onto which the desired circuit pattern can be formed photographically. The completed stencil has open mesh determined by the pattern exposed on the sensitized screen through which the desired pattern can be printed. The stencil is held in position at a distance of around 0.5 mm from the top surface of the substrate which is adjustable. The ink (paste) is then placed on the opposite side of the screen and a squeegee traverses the screen under pressure which transfers the thick film ink onto substrate in a defined pattern. Consequently, the required wet circuit pattern is left on the substrate to promote print leveling for 5-10 minutes [Ivanov (2004)].

The next step is to dry the film and remove the organic solvents from the paste in an oven at a temperature range of 100-125 °C. The dried film is relatively immune to smudging and the substrates can be handled. The drying step is followed by the firing step in which the previously dried films are exposed to high temperatures to form a solid, composite material and acquire all its electrical properties. This is usually done in a conveyer belt furnace, where parameters like peak temperature, dwell time and throughput speed can be controlled as per the required profile of a specific paste. All thick-film inks (pastes) contain glass frit which melts during the firing cycle and forms a mechanical key at the film-to-substrate interface. It also provides a suitable glass matrix for the active material of the film resulting in a

composite film, which is firmly and permanently bonded to the substrate. Further screen-printed layers may be added after firing if necessary [Ivanov (2004)]. The process of fabrication of thick film gas sensor array followed in the present work is shown in Fig 2.11.

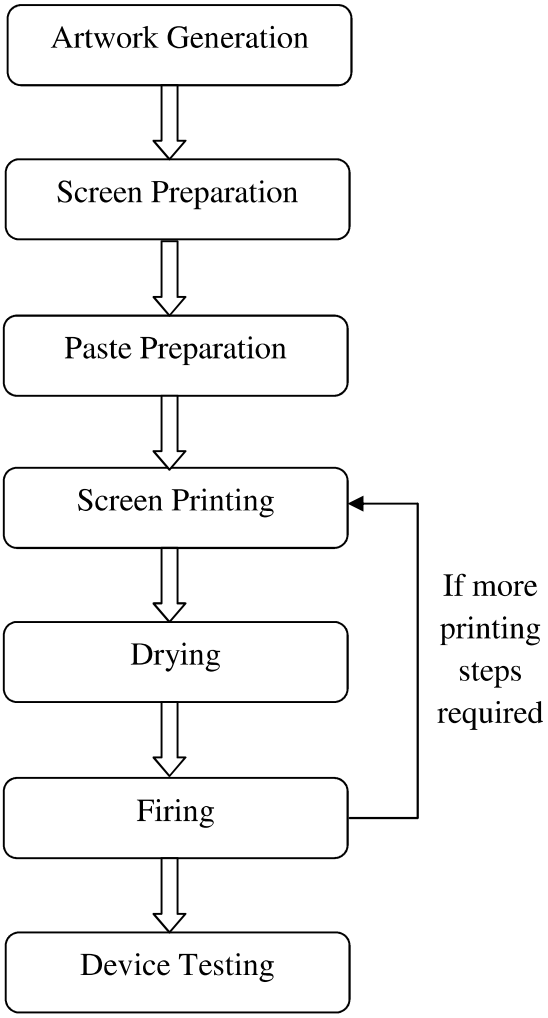

Fig. 2.11 Flow chart for thick film sensor array fabrication

2.4.1 Artwork Generation for Sensor Array

In earlier days, generating the artwork for thick-film screens was a very time consuming task, since the master pattern was produced by traditional methods such as tape strips and decals, drawing and inking, cut-and-peel techniques with materials like Rubylith and Stabilene. Though these methods have their own advantages, but generally, it is difficult to achieve sharp edges, positional accuracy and uniform density. In the modern advanced computer world, the systems have excellent graphic

facilities which allow a variety of input devices to be used. There are many commercially available software drawing packages (Cadence, Corel draw etc.) which facilitate to produce computer-generated artwork in a fraction of the time as and when needed.

Once the design has been completed on a suitable software package with suitable design rules the next phase in the design process is to generate a hard copy of the design. The exact form of this copy can take one of several forms depending on the equipment used. Nowadays, with the advent of accurate photo-plotters, it is possible to take the layout and accurately reproduce it on photographic film directly, so that it can be developed and fixed ready for screen manufacture.

The pattern for printing stages of fabricated thick film sensor array with common electrode pattern is shown in Fig. 2.12. The geometrical details are given in Table 2.2.

Table 2.2 The geometrical details of fabricated thick film sensor array

Parameters	Integrated Sensor array (mm)
Length of electrode fingers	6
Width of electrode fingers	3
Inter-electrode spacing	0.6
Sensing Area for Each Sensor	4.25 x 7

2.4.2 Screen Preparation

Screen preparation is an important step in the thick film device fabrication. The screen allows the transfer of ink (paste) through a fabric screen on to a substrate. This transfer occurs when the paste comes into the contact with surface and is pulled though the screen. Generally, the screen consists of a frame of cast aluminum, onto which a finely woven mesh is stretched. The mesh itself is usually based on a plain weave pattern as shown in Fig. 2.13. It has some important properties viz. size and density of the strands (usually quoted in terms of lines per inch), the tension, the orientation and the material. The selection of a suitable mesh count for a screen is a very important criterion which depends on pattern and the type of paste being used. For general-purpose work, a typical mesh count might be 200 strands per inch. The mesh opening provides means of controlling the thickness of the deposit which consequently depends on the mesh count and the filament diameter.

For a given mesh count, the smaller the filament diameter, the larger the mesh opening, so a greater volume of ink will be deposited onto the substrate. The common materials used for thick-film screen meshes are: Polyester, Nylon and Stainless steel. They all have their own advantages and disadvantages but they must meet some fundamental requirements for all screen fabrics.

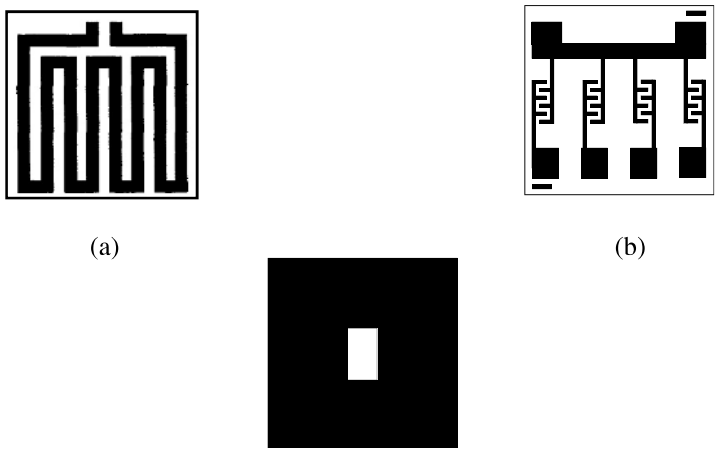

Fig. 2.12 Patterns for fabricating sensor array (a) Heater (b) Interdigitated electrode (c) Sensor patterning mask

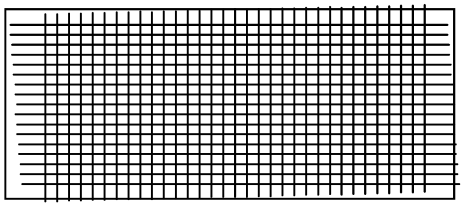

Fig. 2.13 Schematic diagram of mesh of screen

Since the screen acts as a metering device to control print thickness, the mesh material must make sure that the printed deposit is uniform. The mesh material must be precisely woven and have uniform mesh apertures and the fabric should also be flexible enough to enable good contact all over the substrate. The fabric needs to be resilient so that the mesh returns to its original position after the printing stroke. The squeegee itself is in contact with the fabric for most of the printing stroke, so the finish of the fabric must be slippery and smooth so that the resistance to the squeegee

is minimum. The mesh material must also be chemically stable, economic working lifetime and suitable mechanical support for the emulsion [Ivanov (2004)].
Polyester is one of the common fabrics used for screen fabrication due to its flexibility and it is also much more resilient than nylon and stainless steel. Polyester screens have a long life time and give low squeegee wear.

The screen frames are usually made of cast aluminum and serve to hold the mesh fabric taut, and the stencil firm and in place during printing. The mesh is attached to the frame crimping it around the frame edge. Then, further adhesives can be used when the screen fabric is properly tensioned by stretching in all directions to maintain uniform shape and tension. A tension gauge can be used to measures the deflection over a fixed area with a known applied force. When the tension is correct, the mesh is attached to the frame by adhesive.

Next step is the deposition of light-sensitive emulsion. This can be done by three methods viz. direct emulsion method, indirect film method and direct film method. Direct emulsion is a skilled process which involves directly coating the mesh by hand. In the indirect film method the sensitized emulsion film is attached to a clear sheet of polyester backing. The photographic positive is exposed to the emulsion under ultra violet light, washed and then carefully pressed onto the underside of the screen using a soft roller. Emulsion is then allowed to dry for few hours. The polyester backing can be removed and the screen is ready to be used.

In the present work, direct method has been utilized. A1-Emulsion screen printing emulsion manufactured by Photokina Company is mixed with Potassium Dichromate which makes the emulsion light sensitive. The photopositive must be of high contrast and definition. Exposure usually takes place in a special cabinet, with a ultra-violet light source of such a wavelength that the screen emulsion polymerizes. Exposure time is a function of the intensity of the UV source, distance between the light and the screen, the type and thickness of the screen emulsion and the type of pattern being produced [Ivanov (2004); Chaudhary (2013)]. Fig. 2.14 shows the photo images of manual screen preparation tool and the screen prepared using the methods described.

(a) (b)

Fig. 2.14 (a) Manual screen preparation tool (b) Prepared screens

2.4.3 Substrate

The substrate material needs to be robust, and the thermal conductivity should be normally high with very low electrical conductivity. Also, it must be easily shaped, but stable at firing temperatures as high as 900-1000°C. Classically, alumina has been used for this purpose. For normal electronic purposes, the substrate structure is a rectangle that can be mounted in a standard package. Substrates mainly provide the mechanical support and electrical insulation for thick-film hybrid devices. The substrate can affect both the processes and the final characteristics of the devices.

Table 2.3 Some important material characteristics of Al_2O_3 substrate [Topfer (1971)]

Parameter	Specification
Thermal conductivity	0.084 cal/cm-sec°C (25 °C)
Thermal Expansion	6.4×10^{-6} linear coefficient of 25-300 °C
Dielectric Strength	550 Volts/mil (0.025 inch thick)
Dielectric constant	9.1 (25 °C, 1MHz)
Dissipation factor	0.0003 (25 °C, 1MHz)
Hardness	78 Rockwell 45 N
Surface gravity	3.7
Surface quality	15 RMS micro inches
Volume resistivity	104 ohm-cm (25 °C)

Alumina is the most suitable material for thick-film substrates because it combines suitable physical and chemical properties with economic advantages. The industrial standard is now the 96% Al_2O_3 composition, which is used in approximately 90% of worldwide manufactured circuits. Some important material characteristics of Al_2O_3 as substrate are listed in Table 2.3.

2.4.4 Thick Film Pastes

Different pastes were used for fabrication of the thick film sensors

(i) Heater paste

(ii) Electrode paste

(iii) Tin oxide paste

(iv) Doped tin oxide paste (developed in the laboratory)

Heater paste used for backside heater printing is CERMET Platinum conductor (Type-5545), manufactured by ESL Electro Science, USA. It is a screen printable, dense, fritted platinum coating and can be used on alumina for semiconducting tin oxide sensors for the detection of gases. This material is for thin printing and has TCR characteristics approaching that of bulk platinum. Its calibrated peak firing temperature is 850°C for 10-12 minutes as mentioned in specification file. Conductor paste is used for printing electrode pattern of the sensors. Conductive composition paste (Type-8836) from ESL Electro Science, USA has been used for this purpose. It is a mixed bonded, high conductivity gold conductor for use on alumina. It exhibits excellent adhesion and is well suited for thinner electrode printing. It also has optimum firing temperature 850°C for 10-12 minutes.

Tin oxide paste used to fabricate the sensor devices is SnO_2 conductive composition (type-3050), manufactured by ESL Electro Science, USA which was originally developed for transparent electrode fabrication. The paste contains base SnO_2 material mixed with organic vehicle, glass powder and active ingredient that is intended to dominate the electric and sensing properties of the layer. This tin oxide paste was doped with suitable dopants to improve the selectivity and sensitivity of the sensors for the particular gas species under test.

2.4.5 Doped Tin Oxide Pastes

These doped pastes were prepared by adding 1% Pd, Pt and ZnO by weight in the available SnO_2 paste (Type 3050, Electro Science Lab.) and subsequently thoroughly

ball milled for about 6 hours. The choice of dopants depends on the gas/odor being analyzed and the amount in percentage can be optimized for a particular dopant and the gas under test at given operating temperature [Mishra and Agarwal (1998)].

2.4.6 Deposition Equipment Properties and Screen Printing

Screen-printing is an important step in the thick film technology which distinguishes it from other technologies. In this process the paste is transferred through a fabric screen onto a substrate, as the paste comes into contact with the substrate surface and is pulled through the screen with the help of shear action squeegee. The paste is deposited in a pattern defined by the open areas in the stencil of the screen. Some essential screen printing parameters worth highlighting are as follows [Prudentiati (1994); Ivanov (2004)]:

(a) *Snap off*: It is also called breakaway and is defined as the distance between the bottom of the screen and the top of the substrate surface. This parameter can be set by lowering the screen until it contacts the substrate. The screen is elevated until the bottom is separated from the substrate by a desired distance. Fig. 2.15 describes schematic diagram snap-off.

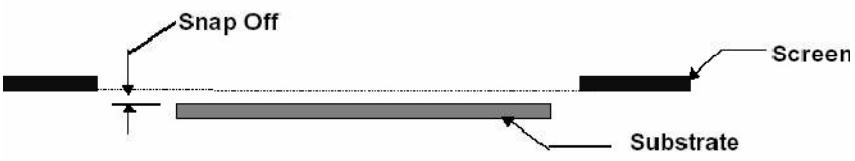

Fig. 2.15 Schematic diagram of snap off process [Ivanov (2004)]

(b) *Attack angle:* This is the angle between the primary edge of the squeegee and the substrate surface. The transfer of the material to the substrate is controlled by this parameter (see Fig. 2.16).

(c) *Squeegee durometer:* This defines the hardness level of the squeegee. Different colors indicate the durometer number. The relation between color and hardness may vary between vendors.

(d) *Squeegee pressure*: This is the force required to push squeegee up from its lowest position in the printing mode.

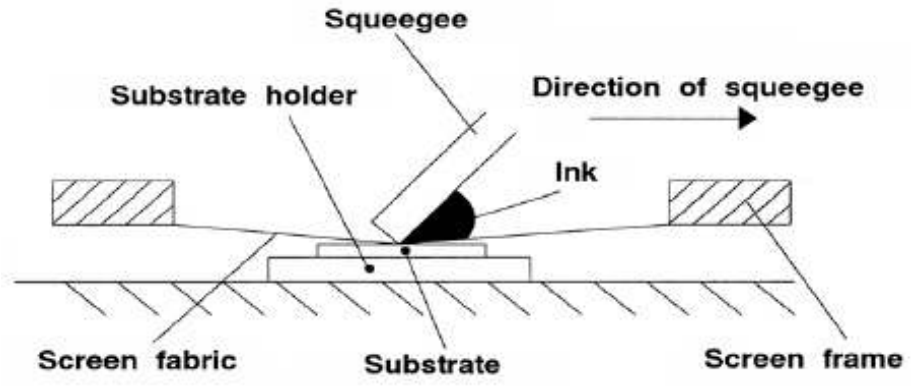

Fig. 2.16 Essential part of a screen printer [Ivanov (2004)]

(e) *Down-stop*: This is the mechanical limit of stopping squeegee travel which is set by lowering the squeegee to come into contact with the substrate.

(f) *Peel:* The release of the screen from the printed area.

(g) *Planarity:* Parallel alignment between the screen and substrate.

The screen is separated from the substrate by small gap which is called snap-off gap which is of around 0.5 mm. The substrate is held in position by the substrate holder. Either a vacuum chuck and by a special jig can be used for this purpose. Since the substrate must be parallel to the screen, it can be adjusted in the vertical plane at both ends. The screen position can be finely adjusted for registration purposes.

The paste material is applied to the upper surface of the screen and the flexible rubber squeegee is traversed across the stencil. While the squeegee is traversing across the screen, the mesh fabric is pressed into contact with substrate surface. The paste is thus forced through the open areas of the screen mesh. Directly behind the squeegee, the screen peels away from the substrate and leaves behind a deposit of paste on the surface of substrate in the required pattern. Fig. 2.17 shows the photograph of screen printing machine.

The angle of attack between the squeegee blade and the screen is generally 45°. The optimum durometer hardness of squeegees is in the range 50-70 [Ivanova (2004)]. It is essential to have accurate control over the squeegee pressure so that print thicknesses are accurate and repeatable.

Fig. 2.17 Photograph of screen printing machine

The squeegee holder is generally floating type *i.e.* pivoted so that it can align itself parallel to the screen. Single direction printing has been adopted as this gives improved registration. One of the most important aspects of thick-film inks is the viscosity, which must be accurately controlled if the quality of the film deposition is to be high. Variation of viscosity of a typical thick-film at different stages during the printing cycle is shown in Fig. 2.18.

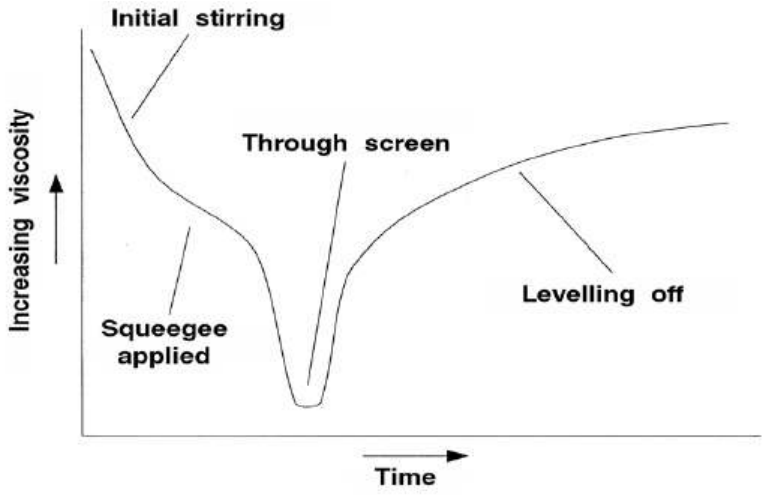

Fig. 2.18 Variation of viscosity of a typical thick-film at different stages during the printing cycle [Prudentiati (1994)]

The *rheology* is the first general requirement that must be considered for thick-film pastes. The characteristics required of the ink viscosity depend on the printing stage. The paste must have low viscosity when it is being forced through the screen.

2.4.7 Monitoring and Controlling Film Thickness

Film thickness is an important parameter which needs to be controlled carefully. There are a number of techniques that can be used for this purpose. Generally it is desirable to measure the thickness at an early stage in the thick-film process so that any errors can be quickly corrected. So, the film should be measured soon after printing or drying. Usually, non-contact measurement methods should be preferred. In the preset work F-20 Film Analyzer from Filmetrics available in the lab has been used for thickness measurement [Internet Resource (IR7)]. Average film thickness of the sensors has been found to be 5.32μm.

2.4.8 Drying and Firing Process

After the film is successfully printed on the alumina substrate, it is allowed to stand in air for a few minutes so that the ink can level off and settle. After this, the inks are subjected to drying process. The purpose of the drying stage is to remove the organic solvents and make the printed film adhere to the substrate and relatively immune to smudging. Drying takes place at temperatures between 100-125 ℃ for 15 to 20 minutes in a conventional box oven as shown in Fig. 2.19

Fig. 2.19 Conventional box oven used for drying process

Firing process is required in order to develop the electrical properties of the thick film paste and also to bond the paste to the substrate permanently. The high temperature firing cycle also removes the remaining organic binders from the film. Each type of thick film paste has its own optimum operating temperature. The electrical properties of some pastes are very sensitive to the firing conditions. Due to this reason accurate control over the processing parameters is needed. Generally the thick-film furnaces are moving belt furnaces containing a number of heating zones. Fig. 2.20 and Fig. 2.21 show the cross section view and photograph of a typical thick film firing furnace respectively.

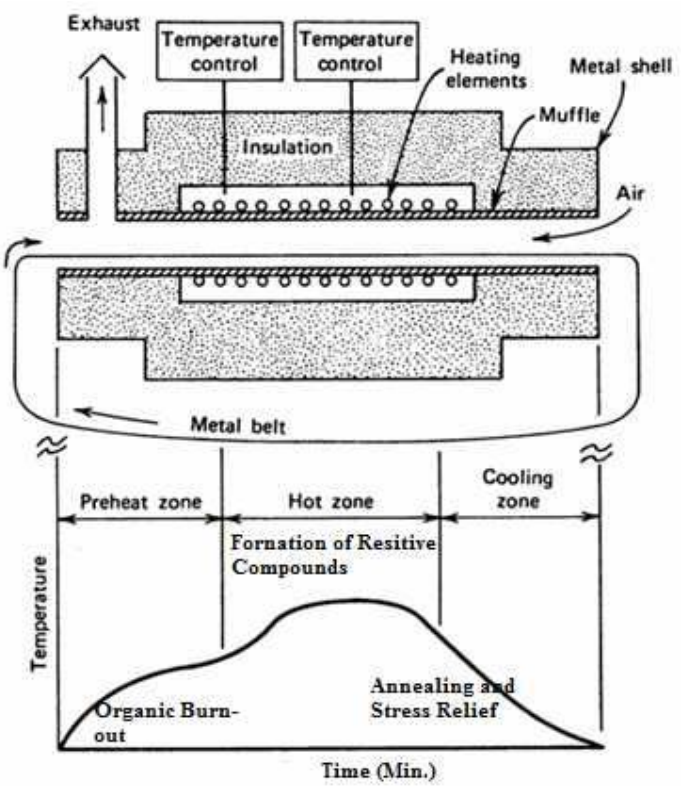

Fig. 2.20 Schematic of cross section of thick film furnace [Internet Resource (IR8)]

Typical firing profile has three distinct regions. In the preheat zone the temperature slowly ramps up towards the peak firing temperature. The temperatures range in this region is 350-400ºC where organics are removed. As the temperature reaches 600-800ºC, the glass frit softens. Glass being an unusual material does not have a definite melting point. It tends to go through a transition stage over a wide temperature range. The second noticeable region is the hot zone where the temperature remains constant

for about 15 minutes. During this time, the active material sinters, various reactions occur and the film acquires all the desired electrical properties. The cooling stage allows the glass to solidify and finally the substrate exits the furnace and stabilizes at the room temperature.

An integrated sensor array was fabricated on a 1'' × 1" alumina substrate. The complete fabrication process was carried out in three steps. In the first step heater was deposited on alumina substrate using a commercial platinum conductor paste (Type-5545, Electro Science Lab, USA) and dried at 120 °C for 10 minutes.

Fig. 2.21 Photograph of thick film furnace

The heater pattern was fired in thick film furnace (DEK Model-840) with total time profile of 40 minutes (15-10-15) with peak temperature zone of 850 °C for 10 minutes. On the other side of the substrate, interdigitated electrode pattern was screen printed using gold conductor paste (Type 8836; Electro Science Lab, USA) and dried at 120 °C for 10 minutes.

The electrode pattern was fired in thick film furnace (DEK Model-840) with total time profile of 40 minutes (15-10-15) with peak temperature zone of 850 °C for 10 minutes. After this, sensing paste was screen printed over a first electrode pattern to make the thick film sensor. The sensor pattern was dried at 120 °C for 15 minutes. When the pattern is hard after drying process, next sensor pattern with different doping was screen printed and then dried again at 120°C for 15 minutes. The process was repeated for all four sensor pattern. It is worth mentioning that the screen, squeegee and spatula etc. must be thoroughly cleaned with suitable chemical (Isoamyl Acetate (pure)) so that unwanted impurities be avoided in the next printing step.

Finally, the screen printed sensor array, after the drying process for 10-15 minutes at 120 °C, was subjected to firing at peak temperature of 550 °C strictly in accordance to the firing profile of the manufacturer (ESL data manual). The images of the fabricated sensor array are shown in Fig. 2.22.

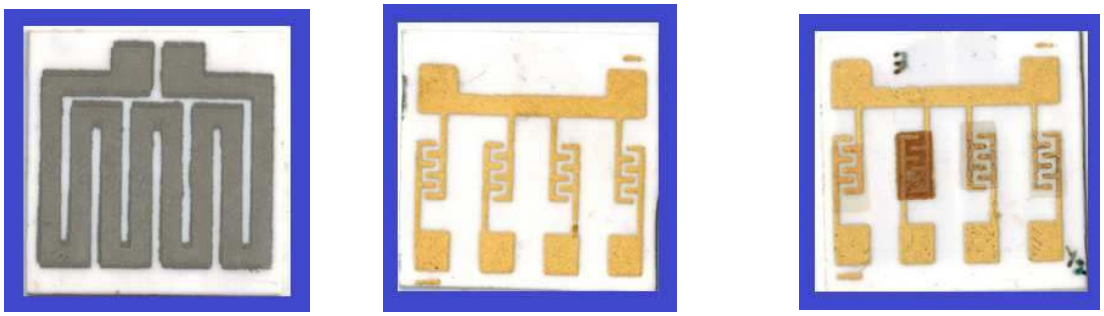

(a) (b) (c)

Fig. 2.22 Photo image of fabricated sensor array (a) Heater, (b) Interdigitated electrodes (c) Fabricated sensor array

2.5 Gas Sensing Properties of Thick Film Gas Sensor

2.5.1 Sensitivity

Sensitivity perceives the variation in the physical and/or chemical properties of the sensing material when exposed to gas. The percentage change in resistance of the sensor is considered as the sensitivity '*S*' of the sensor, *i.e.*

$$S = \frac{R_o - R_g}{R_o} \times 100 \qquad (2.14)$$

where, R_o is the resistance of the sensor in clean air and R_g is the resistance of sensor after the gas exposure. The sensitivity to the individual gases their mixtures of interest must be measured over the whole temperature range so that optimum operating temperature can be determined.

2.5.2 Selectivity

The capacity of a sensor to detect a specific gas in the presence of other gases is called selectivity. The basic problem of SnO_2 gas sensors is that the conductivity value is generally the same for different gas species and concentrations. Another problem is that their responses are very often influenced in the presence of water

vapor. So, any changes in the moisture content of the atmosphere could interfere drastically with the gas sensing properties of the sensors. The sensor selectivity can be improved with use of some sophisticated and extremely expensive techniques. Also, another option could be to increase the active area with nano-metric oxides based film microstructures. Nano-structured materials present new opportunities for enhancing the properties and performance of gas sensors because their surface-to-bulk ratio is higher than that of coarse micro-grained materials.

Selectivity can also be improved by changing the measurement methods in dynamic operation mode such as AC operation mode, modulation of the gas concentration, thermal modulation of the temperature. Another option could be to develop new methods of conditioning and pre-treating of gas mixture before sensing such as catalytic filters to burn out interfering species, use of chromatographic columns [Borjesson *et al.* (1993)] or techniques of selective concentration e. g. carbon traps or polymer-coated fibers.

However, the cross sensitivity of the sensor could be exploited by making use of sensor arrays with pattern recognition techniques which is the most widely used method. This new method is also termed as artificial olfaction whose success depends not only on the development of new sensor technologies, but also on the availability of powerful pattern recognition software. The artificial olfaction instrument, also known as electronic nose (e-nose) instruments are commercially available nowadays and used for assessing quality in the food, beverage and cosmetic industries, etc. The most common approach for fabricating a sensor array is to develop sensors with different dopants as sensing materials for different species of gases/odors [Kohl (1990)].

2.5.3 Response and Recovery Time

The response and recovery time are among the important parameters for assessment of gas sensing behavior of a sensor. The response time (t_{res}) is usually defined as the time required to reach the 90 % of the final steady response value immediately after the injection of the gas in the test chamber. Recovery time t_{rec} is generally defined as the time needed for 90% steady state response of the sensor after the gas exposure is completely removed from the chamber. It is desired that the response time (t_{res}) and recovery time (t_{rec}) values for practical sensor be as small as possible. Good recovery of the sensor enables the sensing device to respond instantaneously in the transient

mode. The response and recovery time can be understood more clearly from the Fig. 2.23.

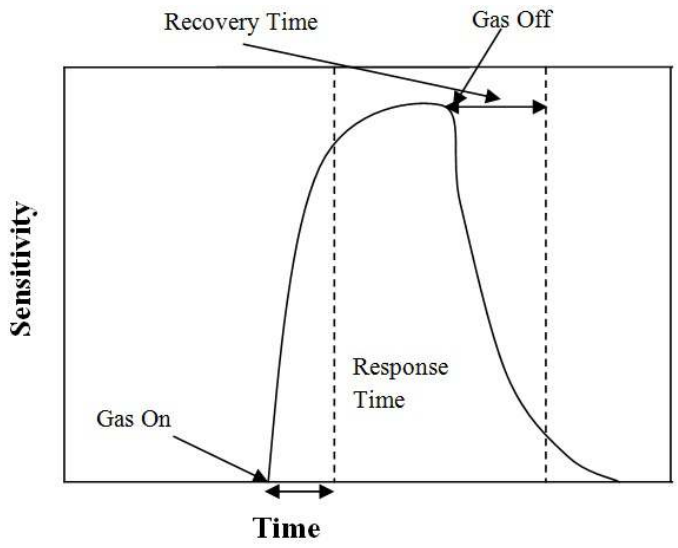

Fig. 2.23 The response and recovery analysis for a thick film sensor

2.5.4 Concentration of the Test Gas

In the present work the variation of sensor response with the gas concentration has been measured in parts per million (ppm). To measure the gas concentration in ppm, following equation has been used

$$Gas\ Concentration\ (ppm) = \frac{Known\ injected\ volume\ of\ gas(in\ litres)}{Volume\ of\ the\ chamber\ (in\ litres)\times 10^{-6}} \quad (2.15)$$

The linearity and the saturation level (sensor range) are obtained by sensitivity curve which is a plot of sensitivity against concentration. The sensor range can also be used to refer either the lowest of detection level of the gas concentration or the smallest increment of the gas increment that can be detected in the sensing environment.

2.6 Electrical Characterization of the Sensor Array

The fabricated sensor array was mounted in the test chamber as mentioned previously. The sensor array was heated to the desired temperature by providing a heater power of 12.76 W (optimized) for generating an operating temperature of 350 °C. The heater power was previously calibrated against temperature using a Ni-Cr thermocouple [Mishra (1996)]. The inlet and outlet of the chamber are closed and the test gas/odor is injected through the rubber septrum provided at the top plate of the test chamber.

The resistance of the sensor is noted at different concentration of the test gases/odors. The percentage change in resistance of the sensor is considered as the sensitivity '*S*' of the sensor, *i.e.*

$$S = \frac{R_o - R_g}{R_o} \times 100 \tag{2.16}$$

where, R_o is the resistance of the sensor in clean air and R_g is the resistance of sensor after the gas exposure. The sensor elements possess the peak sensitivity at an operating temperature of 350 °C. This operating temperature was fixed for further characterization of sensor array. The steady state responses of the sensor array with varying concentration of LPG, N_2O, Acetone and 2-propanol are shown in Fig. 2.25 respectively. The behavior of sensitivity with concentration of test gases is found to be non-linear and is in good agreement with the earlier reported results [Mishra and Agarwal (1998)] which relates the conductance change as follows:

$$G = P_{o2}^{-\beta} \left(1 \sum K_i P_i^{n_i}\right)^{\beta} \tag{2.17}$$

where P_i represents the partial pressures, n_i, the stoichiometric factors and K_i sensitivity coefficients for different gases.

It is evident from the Fig. 2.25 (a)-(d) that the sensitivity of undoped tin oxide sensor is relatively low for all test gases. After addition of metal catalyst like, palladium, platinum and ZnO tin oxide showed significant improvement in the sensitivity for different test gases.

The undoped tin oxide sensor showed very low sensitivity towards LPG. But for N_2O, Acetone and 2-propanol it has shown relatively higher sensitivity as compared to LPG. Pt doped sensor has shown highest sensitivity for for LPG (48%), N_2O (41%) and Acetone (62%). ZnO doped sensor showed highest sensitivity for 2-propanol (64%) and comparable sensitivity for Acetone (60%). The experiment was performed with several samples and the response was found to be similar. However, the response of one such sample for each gas/odor has been shown in Fig. 2.25 (a)-(d).

Thus, the ZnO-doped sensor is found to be a good alternative for Acetone and 2-propanol detection. The Pd-doped sensor showed sensitivity comparable to Pt-doped sensor for LPG, Acetone and N_2O. Pt-doped sensor has shown highest sensitivity towards N_2O. Fig. 2.26 shows the sensitivity response pattern of the sensor

array in presence of LPG, N_2O, Acetone and 2-propanol at 600 ppm concentration of these gases.

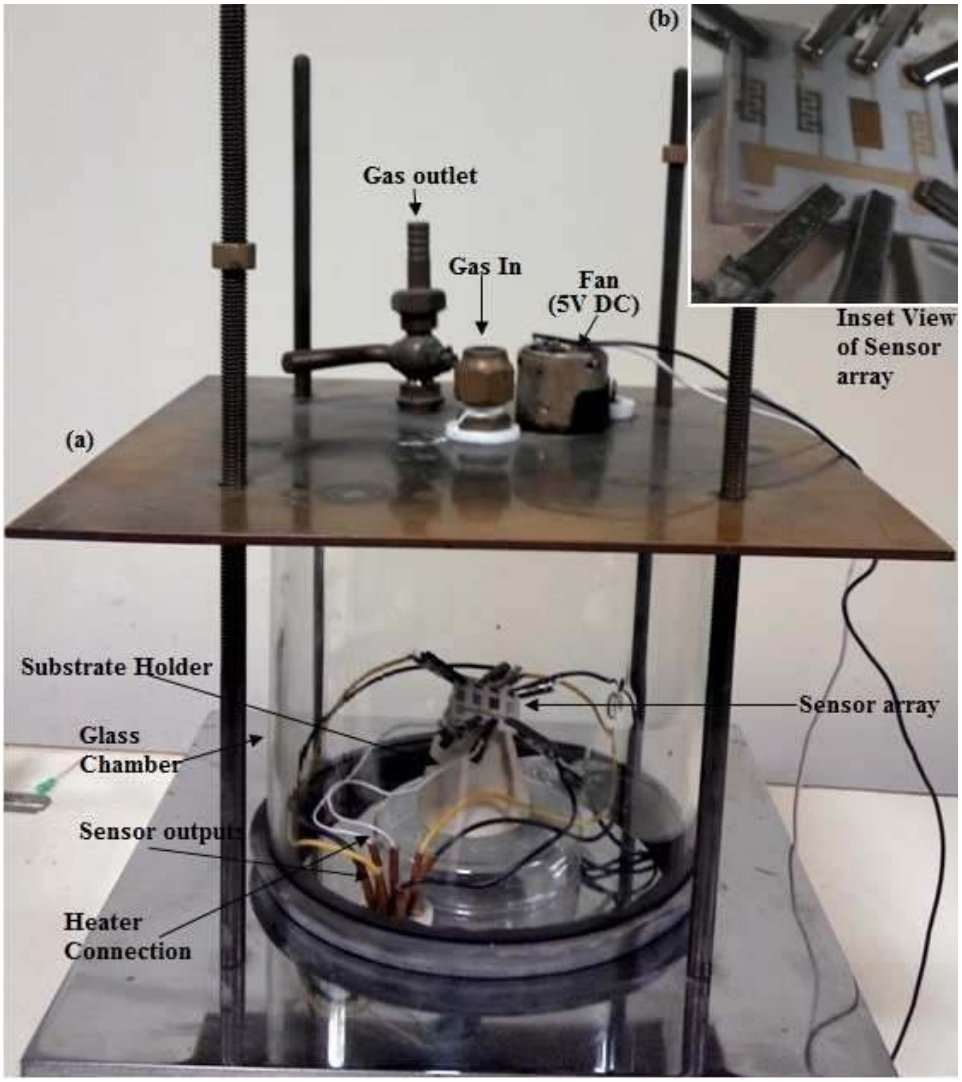

Fig. 2.24 (a) Locally developed test chamber used for sensor array characterization (b) Sensor array connections [in Inset view]

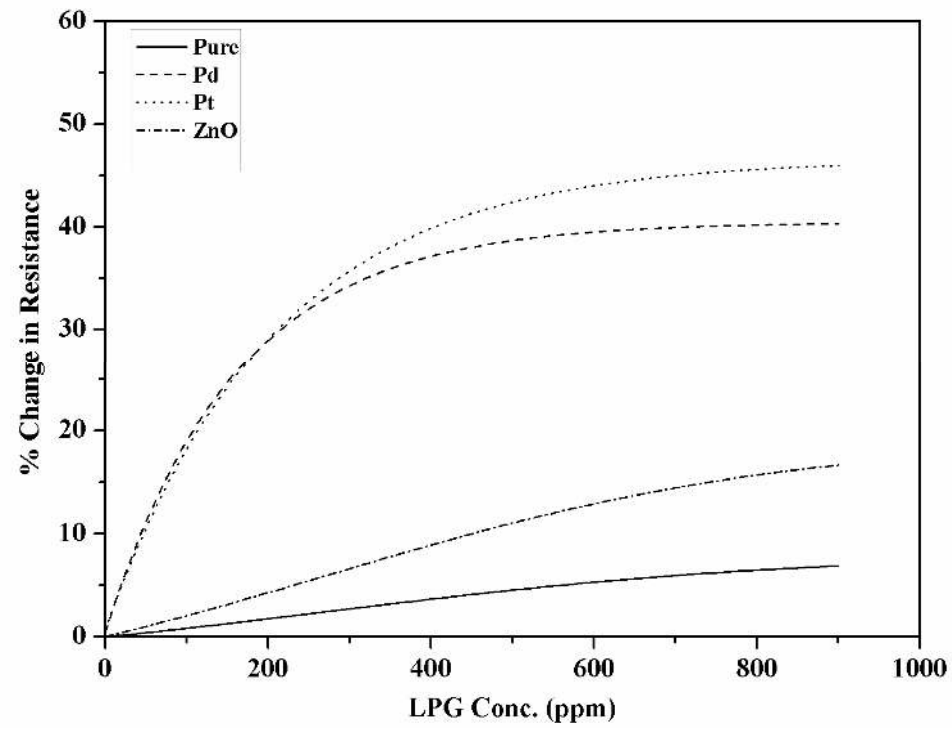

Fig. 2.25 (a) Response graphs of sensor array upon exposure of LPG

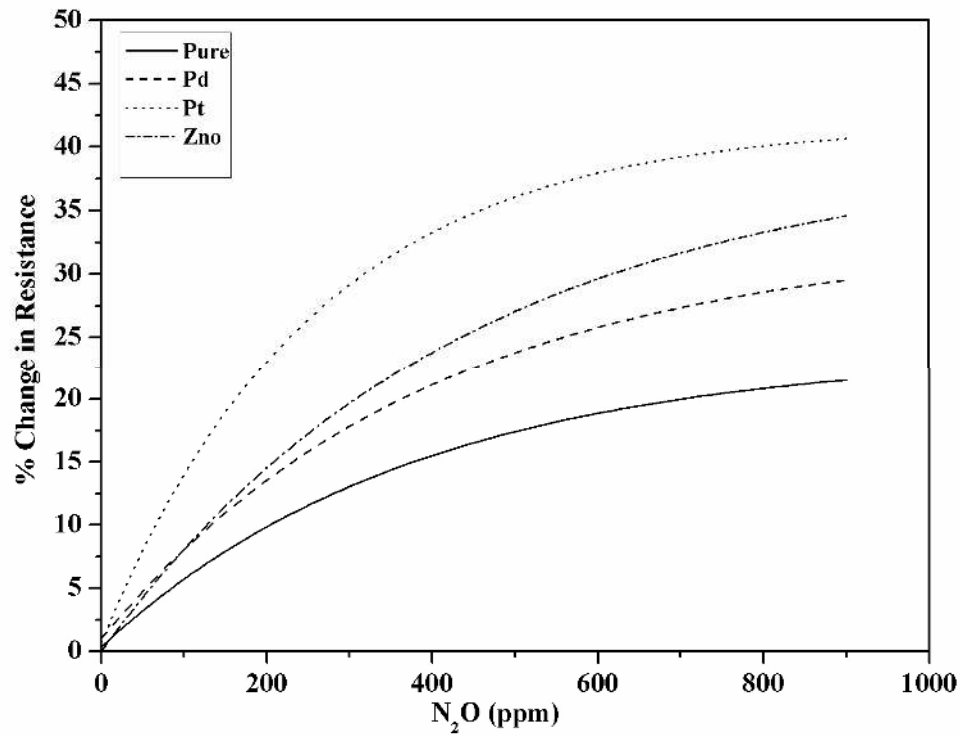

Fig. 2.25 (b) Response graphs of sensor array upon exposure of N_2O

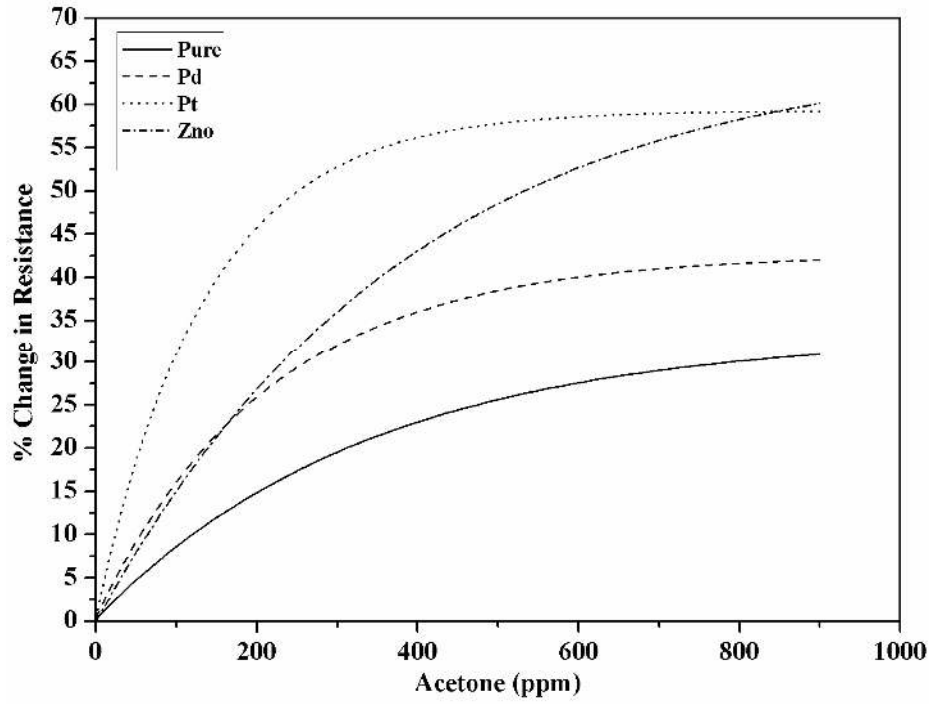

Fig. 2.25 (c) Response graphs of sensor array upon exposure of Acetone

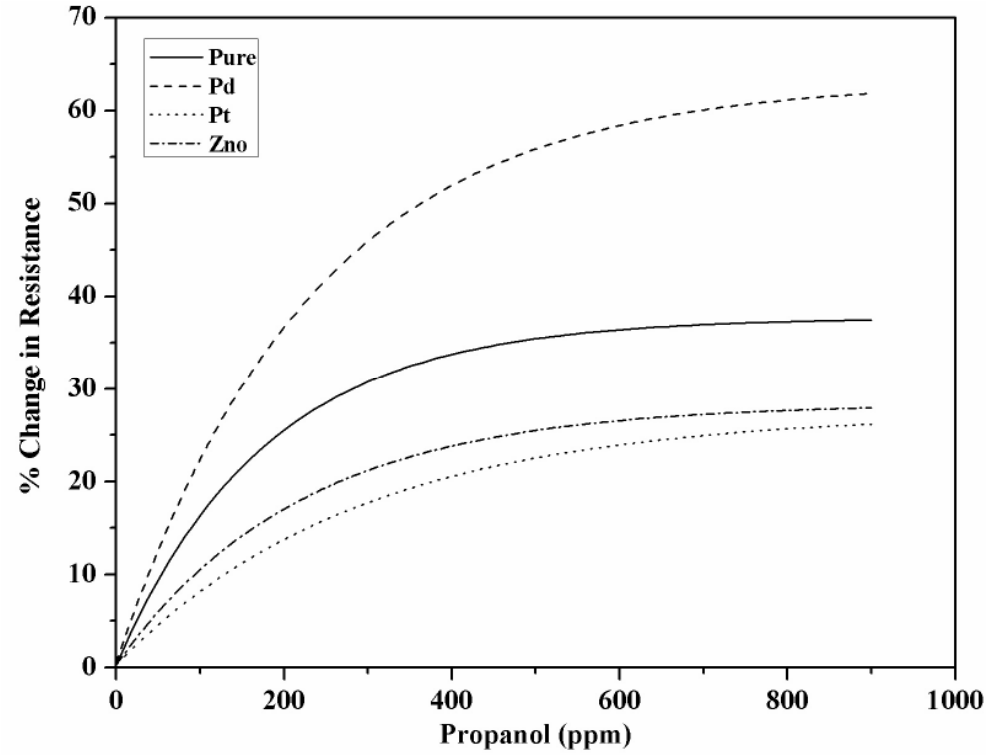

Fig. 2.25 (d) Response graphs of sensor array upon exposure of 2-propanol

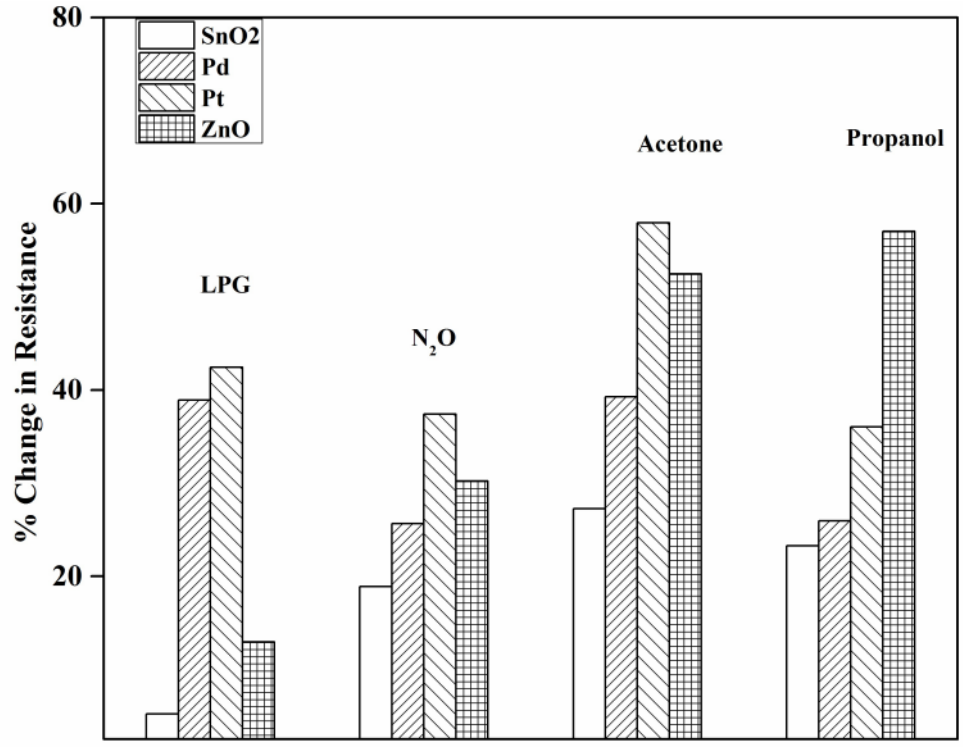

Fig. 2.26 Response bars for sensor array upon exposure of LPG, N_2O, Acetone and 2-propanol at 600 ppm

The response and recovery analysis for each gas/odor was performed with the sensor which showed the highest sensitivity for the respective gas. For LPG, N_2O and Acetone, Pt-doped sensor was used for response–recovery study due to its best response for these gases. Due to the same reason ZnO-doped sensor was chosen for 2-propanol.

Fig. 2.27 (a)-(c) show the sensitivity variation with time of the Pt-doped sensor upon exposure of LPG, N_2O and Fig. 2.27 (d) shows the sensitivity variation with time of ZnO doped sensor upon exposure of 2-propanol at different concentrations. It is obvious from these figures that all response and recovery curves are quite reproducible.

Single response-recovery plot for each test gas is shown in Fig. 2.28. The response and recovery time for each test gas was noted with best responding sensor (Pt-doped in case of LPG, N_2O, Acetone and ZnO-doped in case of 2-propanol) at different concentration values of corresponding gases/odors.

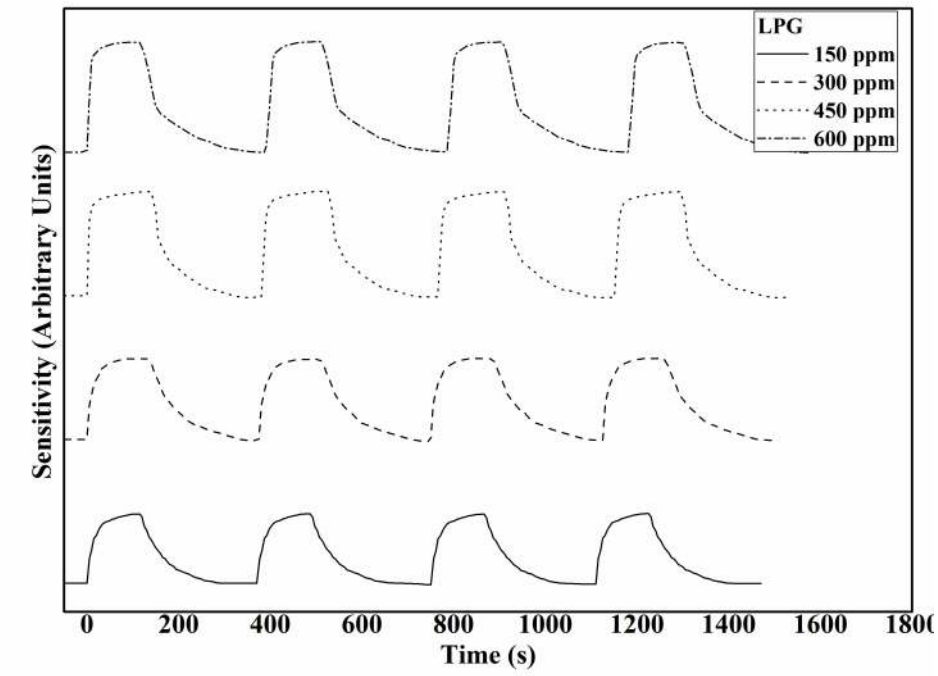

Fig. 2.27 (a) Sensitivity variation with time for LPG

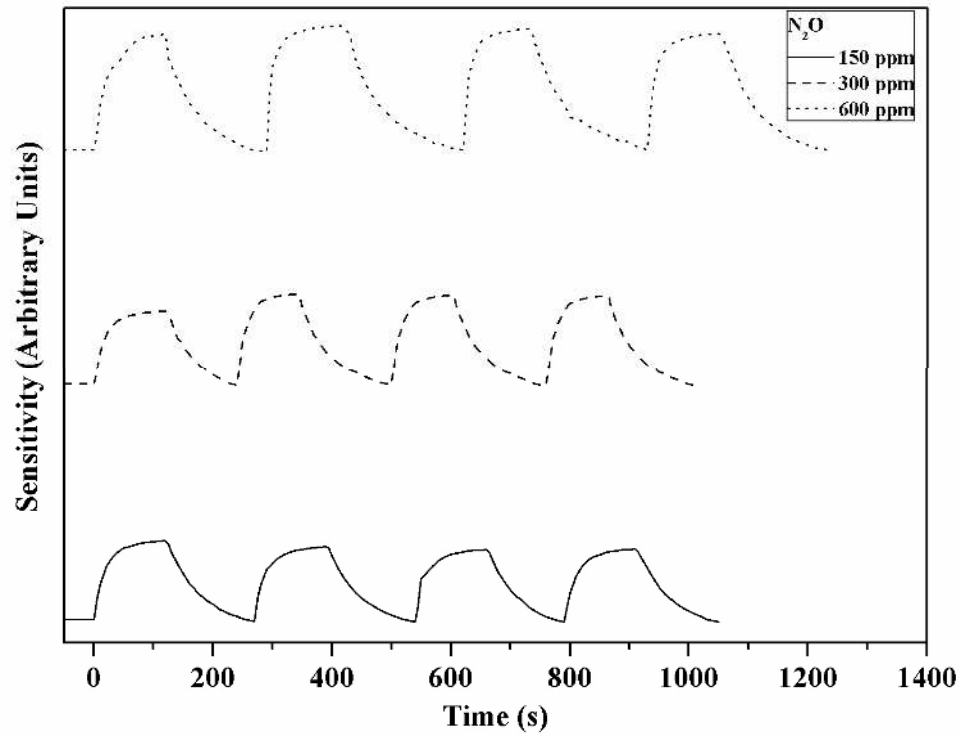

Fig. 2.27 (b) Sensitivity variation with time for N_2O

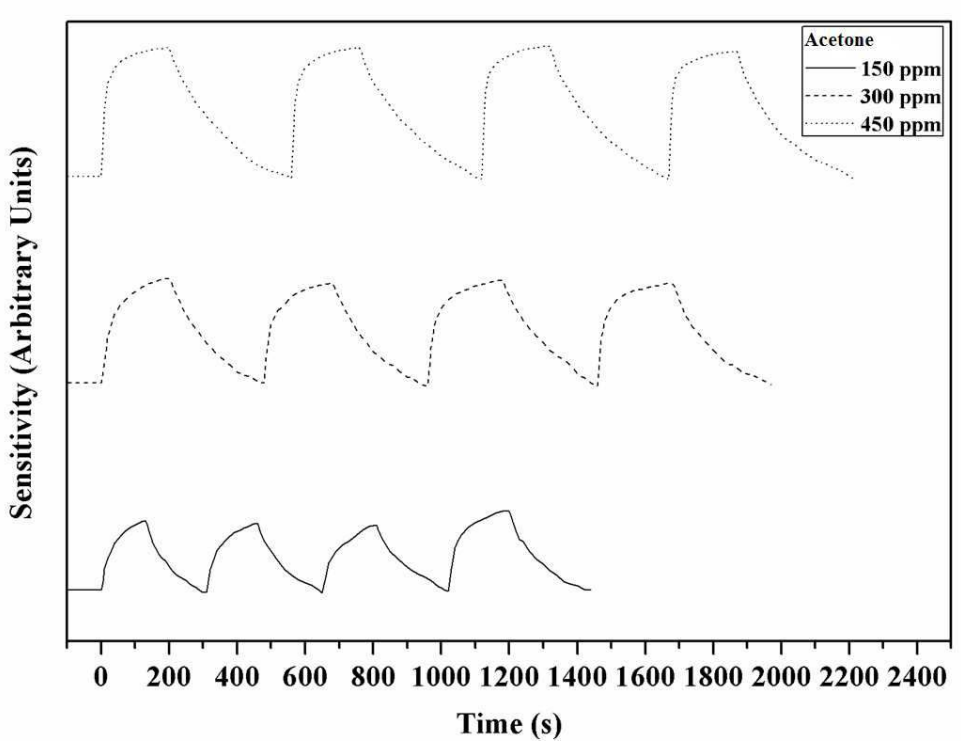

Fig. 2.27 (c) Sensitivity variation with time for Acetone

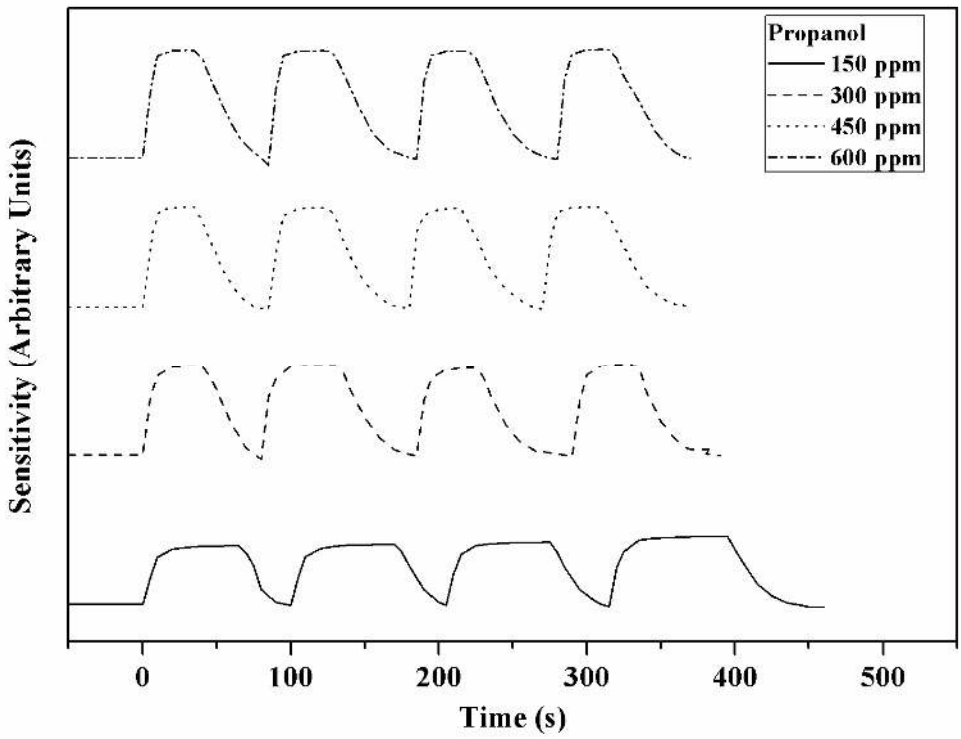

Fig. 2.27 (d) Sensitivity variation with time for 2-propanol

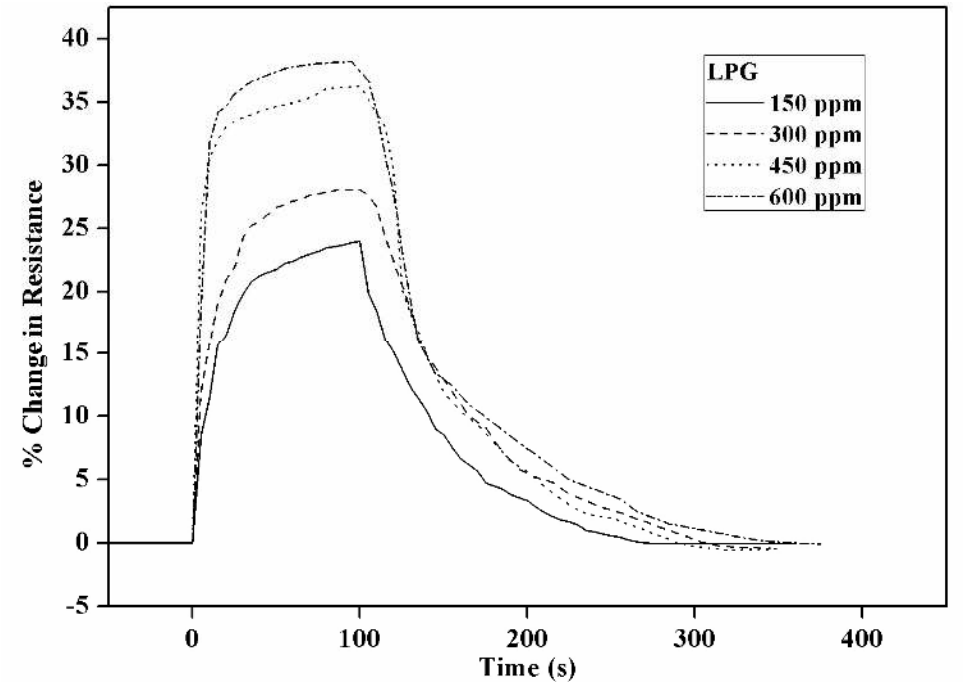

Fig. 2.28 (a) Response and recovery plots for single cycle for LPG

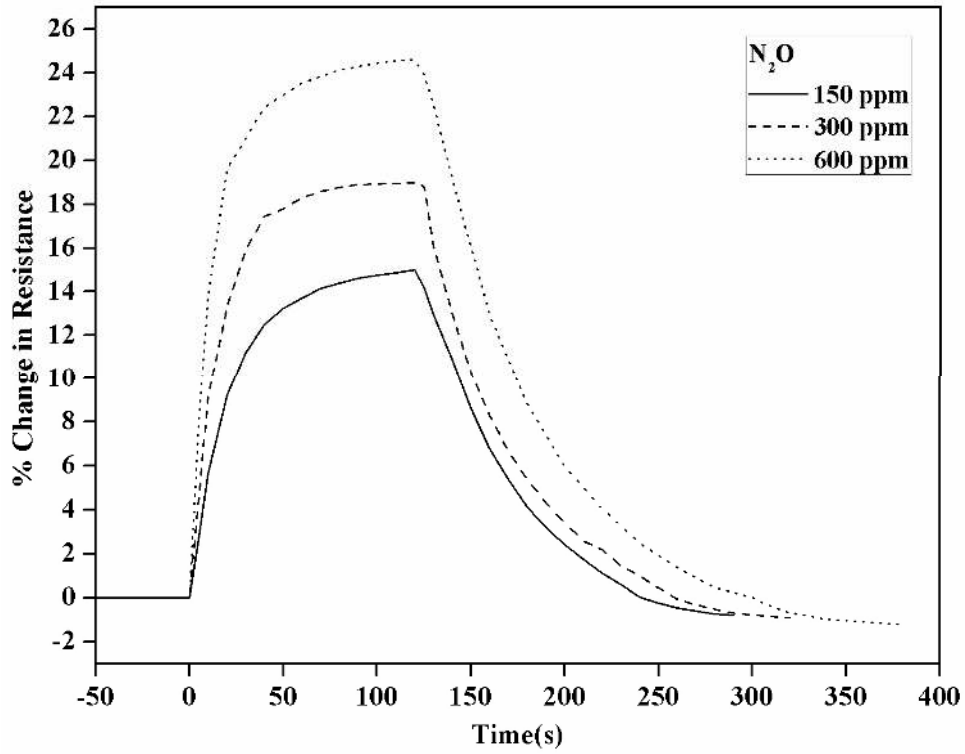

Fig. 2.28 (b) Response and recovery plots for single cycle for N_2O

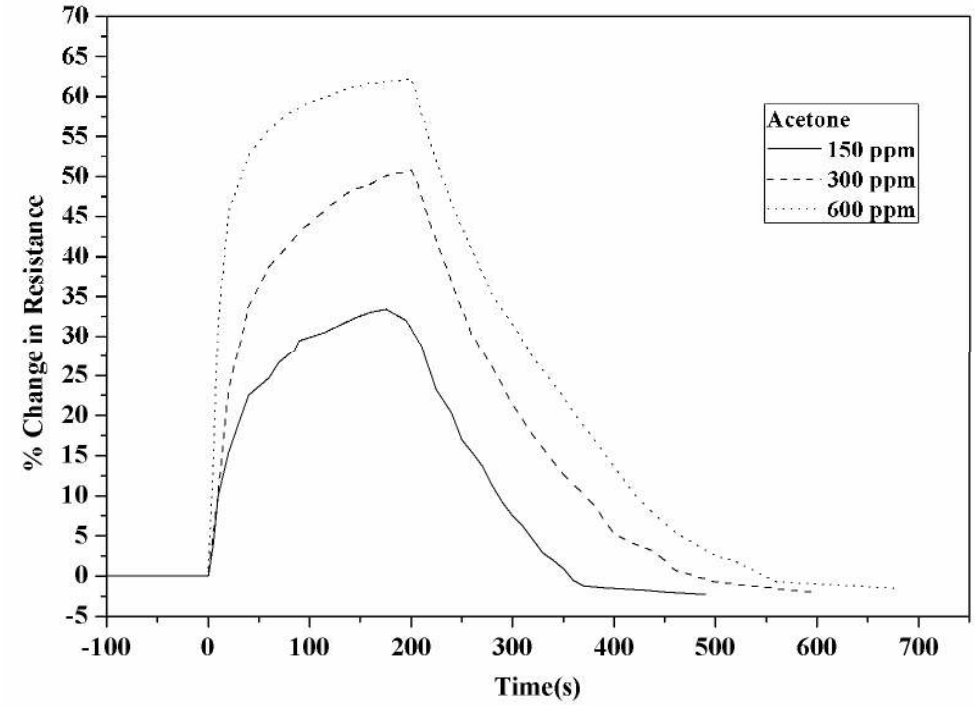

Fig. 2.28 (c) Response and recovery plots for single cycle for Acetone

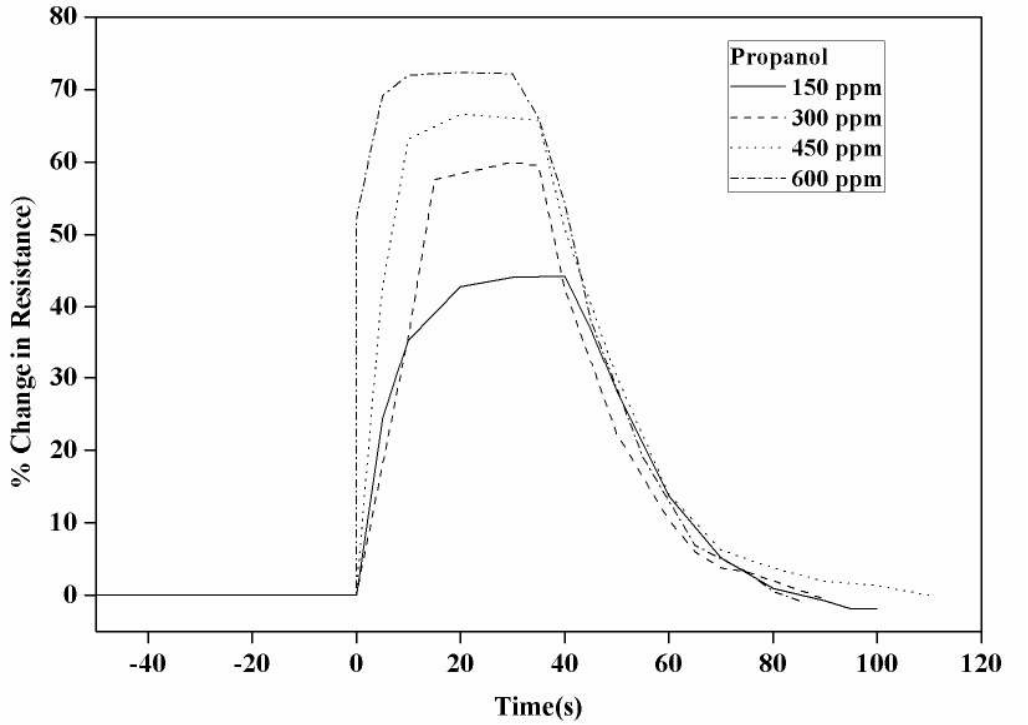

Fig. 2.28 (d) Response and recovery plots for single cycle for 2-propanol

It is evident that the response time is decreasing with increasing the test gas concentration while the recovery time is increasing with concentration which is in good agreement with the results reported in literature [Srivastava *et al.* (2009)].

The transient response of Pt-doped, and ZnO-doped sensors have shown quite reproducible results with small values of response and recovery time. Response time was found to be minimum for 2-propanol (~4 s) for ZnO doped sensor and maximum for Acetone (~58 s) for Pt-doped sensor. The recovery time was found to be minimum for 2-propanol (~44 s) and maximum (~268 s) for Acetone.

2.7 Validation of the Experimental Results

Several models have been proposed to understand the sensing mechanism of tin oxide [Morrision (1982); Geisdinger (1993); Gardner (1990)]. In the present work, rather a general model proposed by Srivastava *et al.* (1994), has been adopted, which defines the behavior of sensor conductance as a function of the concentration of test gas and the operating temperature of the sensor. This model has been used to validate the experimental results.

According to this model, following relation occur between gas conductance (G) and the concentration (C) of the test gas

$$\log[\log(G/G_o)] = \log(B') + b' \log(C) \qquad (2.18)$$

where,

b' = A temperature independent constant;

B' = A parameter which varies with temperature

where, G_o is the conductance of the of the sensor in air. It is evident from the equation (2.18) that a plot of $\log[\log(G/G_o)]$ versus $\log(C)$ is a straight line with slope = b' and intercept = $\log(B')$. More details can be found in [Srivastava *et al.* (1994)]. Using the above expression in equation (2.18), the observed sensitivities of the sensors with concentration were validated for all the four sensors of the array with each test gas and have been shown in Fig 2.30.

It is evident from these plots that the plots between $\log[\log(G/G_o)]$ and $\log(C)$ result in almost straight lines for all sensors at constant operating temperature of 350 °C. Thus, the observed experimental results are in good agreement with the predicted model of sensing mechanism of thick film tin-oxide sensor.

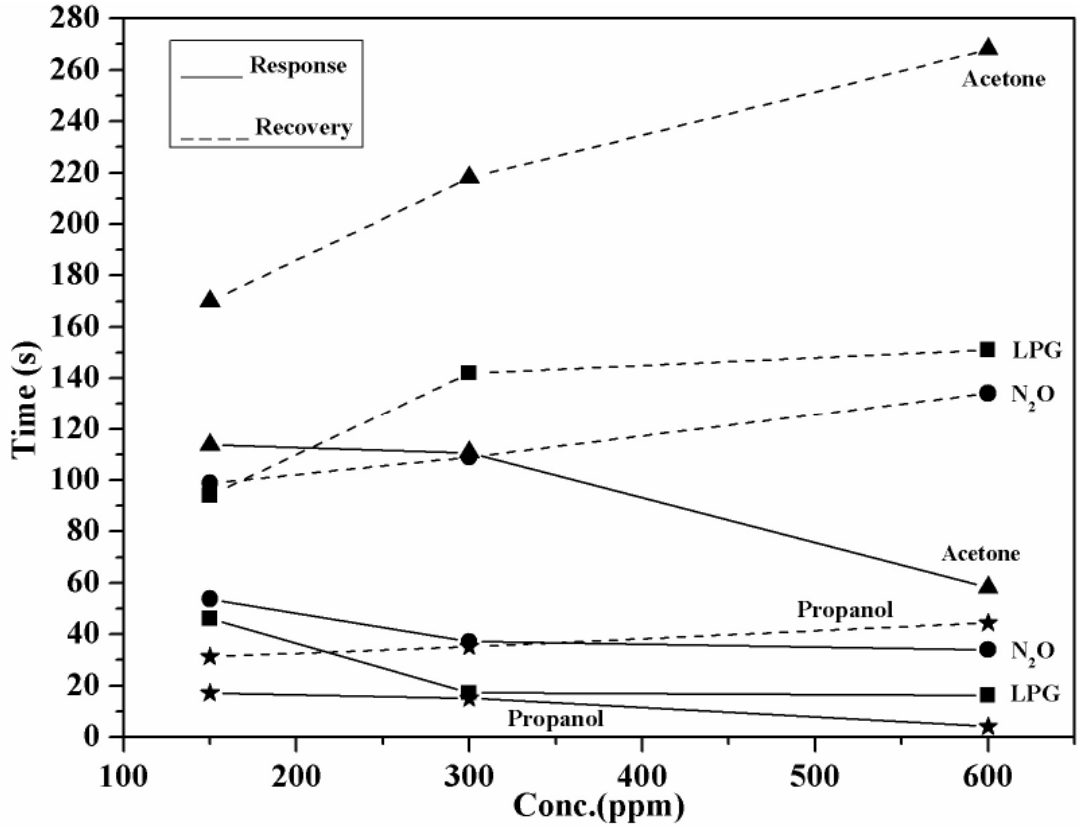

Fig. 2.29 Variation in response and recovery time of sensor with change in concentration of test gas

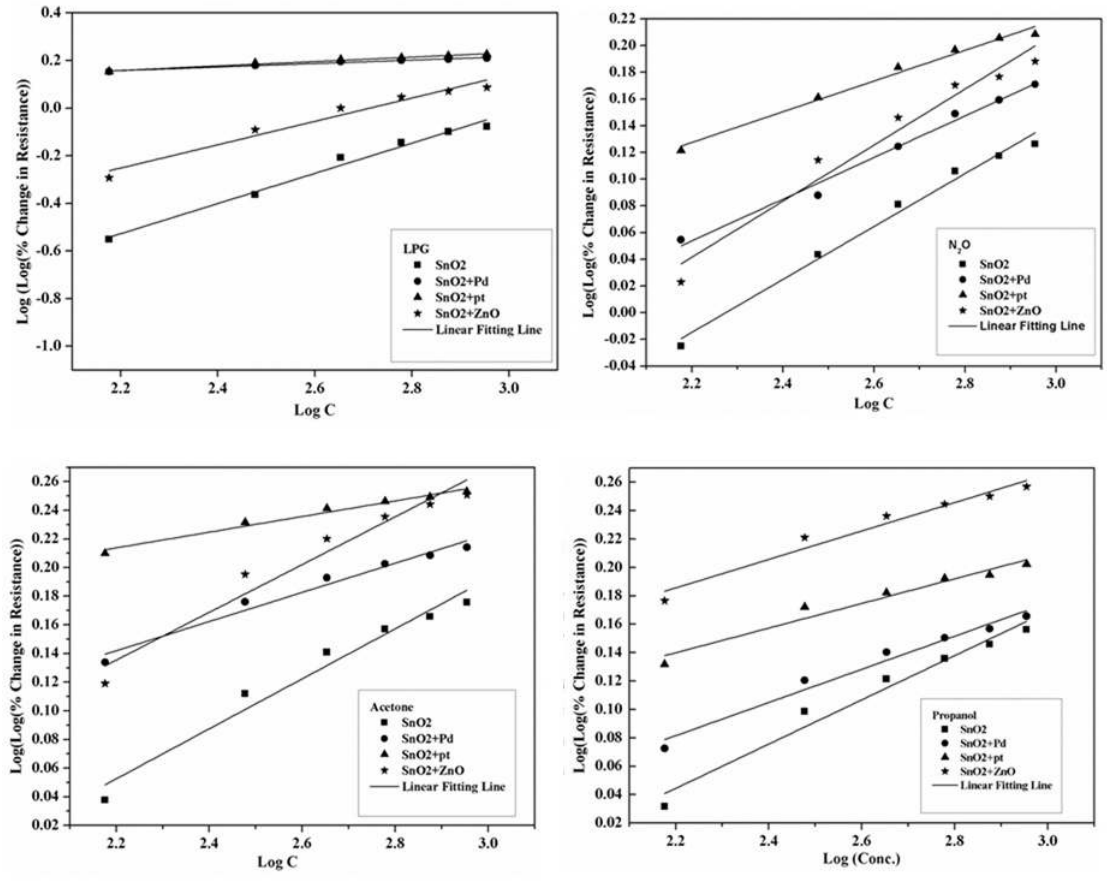

Fig. 2.30 Validation of the experimental results with tin oxide thick film sensor model

2.8 Conclusion

The fabricated integrated sensor array consisting of four sensor element (undoped, Pd-doped, Pt-doped and ZnO-doped tin oxide) has shown different sensitivities to the test gases (LPG, N_2O, Acetone and 2-propanol) and thus suits the input requirements of IGS. The doped sensors have shown good improvement in sensitivity. Even the undoped sensor found to have good sensitivity for some gases like N_2O gas etc. The Pt-doped sensor has shown excellent sensitivity for LPG, N_2O and Acetone. The transient response of Pt-doped, and ZnO-doped sensors have shown quite reproducible results with small values of response and recovery time. Response time was found minimum for 2-propanol for ZnO doped sensor and maximum for Acetone for Pt-doped sensor. The recovery time was found minimum for 2-propanol and maximum for Acetone. The experimental results have been verified with tin oxide thick film gas sensor model and found to be in good agreement at operating temperature of 350 °C. The fabricated sensor array has been utilized for generating

the responses of individual gases/odors and binary mixture of volatile organic compounds and the complete analysis of individual and binary mixture of gases/odors have been discussed in Chapter-3 and Chapter-5 respectively.